PTEP

Prog. Theor. Exp. Phys. **2018**, 043A01 (36 pages)
DOI: 10.1093/ptep/pty038

Emergent symmetries in the canonical tensor model

Dennis Obster[1,2,*] and Naoki Sasakura[2,*]

[1]*Institute for Mathematics, Astrophysics and Particle Physics, Radboud University, Heyendaalseweg 135, 6525 AJ Nijmegen, The Netherlands*
[2]*Yukawa Institute for Theoretical Physics, Kyoto University, Kitashirakawa, Sakyo-ku, Kyoto 606-8502, Japan*
*E-mail: dobster@science.ru.nl; sasakura@yukawa.kyoto-u.ac.jp

Received January 4, 2018; Revised February 15, 2018; Accepted March 1, 2018; Published April 21, 2018

The canonical tensor model (CTM) is a tensor model proposing a classically and quantum mechanically consistent description of gravity, formulated as a first-class constraint system with structural similarities to the ADM formalism of general relativity. The classical CTM produces a general relativistic system in a formal continuum limit, the emergence of which should be explained by the quantum CTM. In this paper we study the symmetry properties of a wave function that exactly solves the quantum constraints of the CTM. We have found that it has strong peaks at configurations invariant under some Lie groups, as predicted by a mechanism described in our previous paper. A surprising result is the preference for configurations invariant not only under Lie groups with positive definite signature, but also with Lorentzian signature. Such symmetries could characterize the global structures of spacetimes, and our results are encouraging towards showing spacetime emergence in the CTM. To verify the asymptotic convergence of the wave function we have also analyzed the asymptotic behavior, which for the most part seems to be well under control.

Subject Index A13, B30, B37

1. Introduction

The current standard model of particle physics describes three of the fundamental forces with great precision. Perturbative methods in quantum field theory are used to calculate scattering amplitudes of processes. The notable absentee in this description of fundamental physics is gravity. The absence of gravity is due to the perturbative non-renormalizability of Einstein's general relativity [1], making the perturbative theory lose its predictive power. Ever since there have been attempts to develop well defined non-perturbative theories that lead to general relativity in some continuum limit.

One way to treat quantum gravity non-perturbatively is by introducing a discretization of spacetime by means of simplices at the Planck scale. One of the ways to do this is by the use of tensor models [2–4], which can be seen as a generalization of matrix models. These original models are known to have some difficulties,[1] some of which have been resolved by the advent of the colored tensor models [7]. However, there still remain problems due to the emergence of branched polymers instead

[1] A serious problem of tensor models with symmetric tensors like the original models is that it is unknown whether there exist $1/N$ expansions that would enable systematic analysis. Recently, introducing a traceless condition [5] or a pair of symmetric tensors [6] have been proposed as possible resolutions.

Funded by SCOAP[3]

of space-like simplicial complexes resembling our universe[2] [10,11]. The problem here may lie in the fact that tensor models usually by construction generate Euclidean signature spaces, without paying special attention to time. One model that treats time differently is causal dynamical triangulation and it is able to produce macroscopic spaces using a notion of causality to restrict generated spaces to be compatible with a (3+1)-dimensional Lorentzian decomposition [12,13]. On the other hand, the Euclidean counterpart (dynamical triangulation) has proved to be more difficult [14,15].

The issues of the tensor models above and the suggestion of the importance of the treatment of time in quantum gravity led to a model called the canonical tensor model (CTM), which was introduced by one of the authors of this paper [16]. The model is defined in the Hamiltonian (also called the canonical) formalism, which naturally treats time separately. Like the Hamiltonian formulation of general relativity (the Arnowitt–Deser–Misner (ADM) formalism [17]), the Hamiltonian consists of a linear combination of first-class constraints. This makes sure that, even though time is singled out, general covariance is not broken. The fundamental dynamical variables of the model are a conjugate pair of real symmetric rank-3 tensors. The CTM has been shown to have a strong connection to general relativity: It agrees with a mini-superspace approximation for $N = 1$ [18],[3] while in a formal continuum limit, where $N \to \infty$, the dynamical structure agrees with that of general relativity [19,20]. Due to this connection with general relativity and the fact that the model can be quantized easily [21], one can hope for this model to be a consistent model for quantum gravity.

Since the main goal of the CTM is to describe quantum gravity, it is important to study the quantum mechanical dynamics of the model, e.g., the physical states (wave functions) [21,22]. One important question is what the properties of the preferred configurations of the wave functions are. Symmetries are especially interesting to analyze since they might give a hint to what kind of spaces can emerge from the model. In this paper we analyze these preferred configurations of a wave function of the model that is valid for general N, particularly paying attention to the mechanism described before in Ref. [23], where configurations that are themselves invariant under a subgroup of the full symmetry group of a system get amplified.[4] We find that this mechanism seems to work well for this wave function of the CTM, observing clear preferences for symmetric configurations. Rather surprisingly, we found not only Lie groups with space-like (positive definite) signatures, but also with spacetime-like (indefinite) signatures, explicitly $SO(1, N-1)$ for the particular simplified cases we consider, as the symmetries associated with the preferred configurations. This suggests that there is a hidden time direction present in the emergent symmetry, possibly signaling the emergence of de Sitter-like spacetimes in the CTM.[5]

This paper is organized as follows. In Sect. 2, we review the formalism of the CTM and present the wave function that we analyze. The wave function is expressed as a holomorphic integration over N variables, which can be seen as a multi-variable generalization of the Airy function. In Sect. 3,

[2] Recently, tensor models have been attracting much attention as Sachdev–Ye–Kitaev (SYK)-like models without disorder [8,9]. In this context, tensor models may be indirectly related to quantum gravity through holography, in which the dominance of branched polymer-like graphs, the so-called melonic diagrams, is important in the exact solvability of the model in the large-N limit.

[3] Here, N denotes the range of the indices of the tensors, namely $1, 2, \ldots, N$.

[4] The main point of this mechanism is that the physical quantity describing a state in the system is invariant under a group G, whereas certain configurations can themselves be invariant under a subgroup $H \subset G$. It was found that these configurations will be greatly preferred over non-symmetric configurations.

[5] Some discretion with this statement is in order here. Though the appearance of such spacetime symmetries is encouraging, a correct geometrical interpretation is still left for later study.

we review the mechanism of the amplification of the wave function at symmetric configurations, which was described in our previous paper [23]. In Sect. 4, we explain the method by which we numerically evaluate the wave function for generic configurations. Since the integrand is oscillatory (oscillating infinitely fast at infinity) with a constant modulus we introduce a regularization procedure, which in physics is often called the ϵ-prescription, to properly handle the conditionally convergent integral. Then, we take the vanishing limit of the regularization by considering a deformation of the integration contour. We introduce a numerical method that takes care of the deformation. In Sect. 5, we consider a subspace of the configurations, in which one can analytically carry out all the integrations except for one. This simplified model is useful for studying the amplification mechanism, especially for large-N cases, because just one integration remains to be evaluated numerically for any N. We observe strong amplification of the wave function at symmetric configurations. We also study the large-N behavior of the wave function. In Sect. 6 we show how the space-like symmetries that are highlighted are promoted to spacetime-like symmetries in this wave function. In Sect. 7, we study the asymptotic behavior of the wave function at the infinity of the configuration space, numerically and analytically. We find a rich variety of possibilities, which should be studied more thoroughly in the future. The final section is devoted to a summary and future problems.

2. Review of the canonical tensor model

The canonical tensor model (CTM) is a model for gravity in the canonical (Hamiltonian) framework, which seems to be a natural starting point to construct a model that treats time differently. There have been several attempts to do this by starting from the ADM formalism [17] of general relativity, where it is described as a first-class constrained system with the fundamental fields being the spatial metric h_{ij} and its conjugate momentum π^{ij}. The (reduced) Hamiltonian density $\mathcal{H}$ is given by a linear combination of the so-called "Hamiltonian constraint" $\mathcal{H}$ and the "(spatial) diffeomorphism constraint" $\mathcal{H}_i$,[6] where the lapse function N and the shift vector N^i act like the corresponding Lagrange multipliers:[7]

$$\mathcal{H} = N\mathcal{H} + N^i\mathcal{H}_i, \tag{1}$$

where the repeated indices are assumed to be summed over. This standard convention will also be assumed hereafter unless otherwise stated. The constraints span the *hypersurface deformation algebra*,

$$\begin{aligned} \{H(f), H(f')\} &= \vec{H}(\vec{F}), \\ \{\vec{H}(\vec{f}), H(f)\} &= H(\mathcal{L}_{\vec{f}} f), \\ \{\vec{H}(\vec{f}), \vec{H}(\vec{f}')\} &= \vec{H}(\mathcal{L}_{\vec{f}} \vec{f}'), \end{aligned} \tag{2}$$

where $\vec{H}(\vec{f}) = \int d^3x f^i \mathcal{H}_i$, $H(f) = \int d^3x f \mathcal{H}$, $F^i = h^{ij}(f\partial_j f' - f'\partial_j f)$, and $\mathcal{L}_{\vec{f}}$ is the Lie derivative with respect to $\vec{f}$.

[6] The diffeomorphism constraint is also often called the momentum constraint.
[7] For a geometric overview of these quantities, see, for instance, Ref. [24].

The most straightforward way to attempt to construct a canonical quantum gravity theory is to quantize the fundamental fields by mapping $h_{ij} \to \hat{h}_{ij}$ and $\pi^{ij} \to \hat{\pi}^{ij}$.[8] Since $\mathcal{H}$ and $\mathcal{H}_i$ are classical constraints, one can implement them on the quantum level by demanding

$$\hat{\mathcal{H}}\,|\Psi\rangle = 0, \tag{3}$$

$$\hat{\mathcal{H}}_i\,|\Psi\rangle = 0. \tag{4}$$

Here, Eq. (3) is called the Wheeler–DeWitt equation. This functional differential equation is in general not well defined, although some attempts have been made to make sense of this. There exist various kinds of difficulties in this approach.

To circumvent these issues in the canonical formalism, one may try to describe a space in a discrete way by a set of "points". In the CTM we choose to implement this already at the classical level, by describing the model as a tensor model. The first non-trivial case to try to construct a Hamiltonian with similar properties to Eq. (1) would be a real symmetric rank-3 tensor model, using a conjugate pair of real symmetric rank-3 tensors, Q_{abc} and P_{abc}, as the fundamental variables with the canonical Poisson algebraic relations,

$$\{Q_{abc}, P_{def}\} = \sum_{\sigma} \delta_{a\sigma_d}\delta_{b\sigma_e}\delta_{c\sigma_f},$$

$$\{Q_{abc}, Q_{def}\} = \{P_{abc}, P_{def}\} = 0, \tag{5}$$

where σ are the permutations of d, e, and f. The labels of the tensors range from 1 to N and label the "points" in the space that we are interested in.[9] The $N \to \infty$ limit is supposed to correspond to a continuous space where the model should coincide with general relativity.[10] Similar to the spatial diffeomorphism invariance in general relativity, we introduce a kinematical $O(N)$ symmetry of the system such that the system is invariant under "relabeling" of the points:

$$Q_{abc} \to L_{aa'}L_{bb'}L_{cc'}Q_{a'b'c'},$$

$$P_{abc} \to L_{aa'}L_{bb'}L_{cc'}P_{a'b'c'}, \tag{6}$$

where L_{ab} are $O(N)$ matrices. The CTM is the minimal of its kind, meaning that we consider a model with just two constraints:

$$H = n_a\mathcal{H}_a + n_{ab}\mathcal{J}_{ab}, \tag{7}$$

where $\mathcal{H}_a$ corresponds to the Hamiltonian constraint and $\mathcal{J}_{ab}$ corresponds to the spatial diffeomorphism constraint in Eq. (1). For convenience, and to maintain the analogy to the ADM formalism, we will abuse this terminology to refer to the CTM constraints from now on. The spatial diffeomorphism

[8] This does not appear to be the best method in canonical quantum gravity and one is better off using Ashtekar variables [25], which led to the loop representations in quantum gravity (loop quantum gravity).

[9] We call them "points", since the formal continuum limit suggests that the labels are mapped to continuous coordinates. The exact implementation of this geometric picture at the discrete level is still not fully understood, as the points should be connected in some way, e.g., by simplices.

[10] It is worth stressing that unlike the usual Euclidean-type tensor models, the spacetime dimension emerging from the CTM is not directly related to the rank of the tensors. This can, for instance, be seen in the actual correspondence in a formal continuum limit [19,20].

constraint of ADM generates diffeomorphisms within a certain timeslice [26]; hence it is natural to take for $\mathcal{J}_{ab}$ the generators of $SO(N)$ transformations that we imposed in Eq. (6):

$$\mathcal{J}_{ab} = \frac{1}{4}(Q_{acd}P_{bcd} - Q_{bcd}P_{acd}), \tag{8}$$

which is antisymmetric, $\mathcal{J}_{ab} = -\mathcal{J}_{ba}$. To specify the classical model, one now has to introduce the Hamiltonian constraint. In analogy with the ADM formalism of general relativity, the algebra spanned by the constraints should close. Furthermore, one can deduce that the terms should be connected, corresponding to the absence of non-local behavior in the ADM algebra (2). This means that, for instance, a term like $Q_{abc}Q_{bcd}Q_{dee}$ is allowed but a term like $Q_{abb}Q_{cde}Q_{cde}$ is not. By considering only terms that are up to the third order in Q and P and even in P,[11] one can prove that there is a unique model described by the following Hamiltonian constraint [27]:

$$\mathcal{H}_a = \frac{1}{2}(P_{abc}P_{bde}Q_{cde} - \lambda\, Q_{abb}), \tag{9}$$

where λ is a real constant. Without loss of generality, the constant can be normalized as $\lambda = 0, \pm 1$ by a rescaling, $Q \to c\,Q$, $P \to P/c$, which keeps Eq. (5). The constraints of Eqs. (8) and (9) span the following algebra, which corresponds to the ADM algebra in a formal continuum limit with $N \to \infty$ [19]:

$$\begin{aligned}
\{\mathcal{H}(\xi^1), \mathcal{H}(\xi^2)\} &= \mathcal{J}\left([\tilde{\xi}^1, \tilde{\xi}^2] + 2\lambda\, \xi^1 \wedge \xi^2\right), \\
\{\mathcal{J}(\eta), \mathcal{H}(\xi)\} &= \mathcal{H}(\eta\xi), \\
\{\mathcal{J}(\eta^1), \mathcal{J}(\eta^2)\} &= \mathcal{J}\left([\eta^1, \eta^2]\right).
\end{aligned} \tag{10}$$

Here $\mathcal{H}(\xi) = \mathcal{H}_a\xi_a$, $\mathcal{J}(\eta) = \mathcal{J}_{ab}\eta_{ab}$, $\tilde{\xi}_{ab} = P_{abc}\xi_c$, $(\xi^1 \wedge \xi^2)_{ab} = \xi^1_a\xi^2_b - \xi^1_b\xi^2_a$, and $[.,.]$ denotes the matrix commutator.

The quantization of the CTM can be done consistently by canonical quantization [21]. Let us map the canonical variables to quantum mechanical operators and the canonical Poisson brackets to quantum mechanical commutators:

$$\begin{aligned}
&Q_{abc} \to \hat{Q}_{abc}, P_{abc} \to \hat{P}_{abc}, \\
&\{Q_{abc}, P_{def}\} \to -i[\hat{Q}_{abc}, \hat{P}_{def}].
\end{aligned} \tag{11}$$

The constraints are now given by the operators

$$\hat{\mathcal{H}}_a = \frac{1}{2}(\hat{P}_{abc}\hat{P}_{bde}\hat{Q}_{cde} - \lambda\hat{Q}_{abb} + i\lambda_H\hat{P}_{abb}), \tag{12}$$

$$\hat{\mathcal{J}}_{ab} = \frac{1}{4}(\hat{Q}_{acd}\hat{P}_{bcd} - \hat{Q}_{bcd}\hat{P}_{acd}). \tag{13}$$

[11] The limitation up to the third order has been put in by hand in order to consider the simplest case, and we do not know whether there exist other consistent Hamiltonian constraints with higher-order terms. Whether it is fair to only consider even terms in P is still an open question; however, it can be somewhat physically motivated as a "time reversal symmetry" condition where $P \to -P$ and $Q \to Q$.

The constant λ_H depends on the ordering of the operators in the first term of the Hamiltonian constraint. However, if one requires the Hamiltonian constraint to be self-adjoint, this constant is fixed to be

$$\lambda_H = \frac{1}{2}(N+2)(N+3). \tag{14}$$

Conveniently, the quantized constraint algebra contains no anomalies: the algebra remains of the same form, as can be checked by explicit computations.

Just like the usual constraints in canonical quantum gravity, Eqs. (3) and (4), we have to impose that the physical states of the theory vanish under the constraints

$$\hat{\mathcal{H}}_a |\Psi\rangle = 0, \tag{15}$$

$$\hat{\mathcal{J}}_{ab} |\Psi\rangle = 0. \tag{16}$$

By choosing a representation, these constraints can be expressed as a set of partial differential equations. This means that the problem is in principle well defined, though the solutions can in general have very complicated forms. Several exact solutions have been found before [21,22], and the main interest of this paper is a wave function in the P representation given by

$$\Psi(P) = \int_{\mathbb{R}^{N+1}} d\phi d\tilde{\phi}\, e^{i(P\phi^3+\phi^2\tilde{\phi}-\frac{4}{27\lambda}\tilde{\phi}^3)}, \tag{17}$$

which gives the wave function of a physical state by

$$\Psi_{\text{phys}}(P) = \Psi(P)^{\frac{\lambda_H}{2}}. \tag{18}$$

Here $\phi = (\phi_1, \phi_2, \ldots, \phi_N) \in \mathbb{R}^N$, $\tilde{\phi} \in \mathbb{R}$ and we use the short-hand notations

$$\begin{aligned} P\phi^3 &= P_{abc}\phi_a\phi_b\phi_c, \\ \phi^2 &= \phi_a\phi_a, \\ d\phi &= \Pi_a d\phi_a. \end{aligned} \tag{19}$$

Though there are several exact solutions known, Eq. (17) has the nice property that it is valid for any N. The derivation of this wave function is given in Appendix A. We will mainly consider the $\lambda > 0$ case, as it appears to be the physically most sensible case. Taking $\lambda \to 0$ (after rescaling $\tilde{\phi} \to |\lambda|^{1/3}\tilde{\phi}$ in Eq. (17)) will lead to problems mentioned in the following paragraph. The case of $\lambda < 0$ is not very interesting as no strong peaks are expected to emerge there, which will be shown in Sect. 4. The wave function with $\lambda > 0$ will in fact be shown to have a rich structure, which can be well understood in terms of the highlighting mechanism of symmetries reviewed in Sect. 3. As discussed in Sect. 7 and Appendix D, the wave function seems asymptotically decaying and normalizable in most of the directions of the $|P| \to \infty$ limit, so it seems reasonable to concentrate our attention mainly on the structure of the peaks in the finite region of P.

As for the $\lambda = 0$ case, another wave function is known that is generally valid for any N in the Q representation [22][12] and is given by

$$\Psi(Q) = \int_{\mathbb{R}^N} d\phi \ (\phi^2)^\alpha e^{iQ\phi^3}, \tag{20}$$

where $\alpha = (N+3)(N-2)/8$. The idea of looking at $\lambda = 0$ seems physically justified, since the λ term in Eq. (12) classically leads to non-local behavior in the formal continuum limit [19,20]. However, as shown in Appendix B, the wave functions, Eq. (17) with $\lambda = 0$ and Eq. (20), have peculiar behavior that would make a sensible interpretation difficult. In short, for $\lambda = 0$, due to the homogeneous nature of the wave functions under the rescaling of P (or Q), the system suffers from an instability of collapsing down to vanishing (or divergent) configurations, namely $P = 0$ (or $Q = \infty$). On the other hand, as we will see, the wave function (17) for $\lambda > 0$ has interesting behavior for finite P, which is potentially of physical importance. Thus $\lambda > 0$ seems to be the only physically sensible choice[13] in the quantum CTM. This also suggests an important future subject of study that the classical dynamics analyzed for $\lambda = 0$ in Refs. [21,22] should be modified from this quantum requirement.

Lastly, we would like to comment on the Lorentzian form that we have particularly taken in Eq. (17); namely the exponent of the integrand has an overall factor i with a real action[14] and the integration region is a real hyper-plane. As reviewed in Appendix A, only the validity of partial integrations is the essential ingredient of the proof for the wave function to be the solution. Therefore, as long as the integration is convergent, one can freely take the overall factor and the integration region: there is no particular reason to take the Lorentzian form from the requirement of physical states. On the other hand, in our treatment of paying special attention to the time direction, the Lorentzian form would be the most natural choice, and moreover it has the following two advantages. One is that, as will be discussed in later sections, the wave function is generally well defined as a conditionally convergent integral for generic P. This will pose more difficult problems in the Euclidean form, as the integral will usually suffer from divergences caused by the cubic terms, unless the integration region is altered to some non-trivial complex one. Another important reason is that the highlighting mechanism of symmetries explained in Sect. 3 requires the coherence/decoherence of the integrand to occur, and the Lorentzian form would be the most efficient one for the mechanism to be evident. Therefore, though it might be theoretically possible to make some other choices, we will exclusively consider the Lorentzian form throughout this paper.

3. Highlighting mechanism of symmetries

In Ref. [23] the authors of this paper introduced a mechanism that can explain the preference for symmetric configurations in models similar to the CTM. This section serves as a short review of this mechanism.

[12] Eq. (20) is a solution to the second-order partial differential equations derived from the Hamiltonian constraints in the Q representation. Therefore, the solution is more non-trivial than Eq. (17) in the P representation, which is a solution to the first-order ones. Unfortunately, we do not presently have any generalization of this solution to $\lambda \neq 0$.

[13] λ corresponds to the cosmological constant in the correspondence between the CTM with $N = 1$ and the mini-superspace treatment of general relativity [18]. Therefore, the necessity of $\lambda > 0$ curiously matches the present astrophysical observation of a positive cosmological constant.

[14] For convenience we use the terminology "action", inspired by the path integral formulation of quantum field theories. The action in Eq. (17) is $S = P\phi^3 + \phi^2\tilde{\phi} - \frac{4}{27\lambda}\tilde{\phi}^3$.

In physics, one is often interested in quantities of the form

$$\Psi(Q) = \int_{\mathcal{C}} d\phi \; e^{iS(\phi,Q)}. \tag{21}$$

Here Ψ is the physical quantity of interest, defined on a configuration space of which Q is an element. ϕ denotes some internal integration variables in the space $\mathcal{C}$ and $S(\phi, Q)$ is a function of ϕ and Q. Note that the wave function (17) of our interest also has this form.

Let us introduce a group symmetry in Eq. (21). Considering Q and ϕ, which are labeled by some discrete set of labels, one can look at the action of some group G on Eq. (21), where Q and ϕ transform under some representations:

$$\begin{aligned} \phi_a^{(g)} &= R(g)_a{}^b \phi_b, \\ Q_i^{(g)} &= \tilde{R}(g)_i{}^j Q_j. \end{aligned} \tag{22}$$

Here, R and $\tilde{R}$ are representations of the group element $g \in G$. Both R and $\tilde{R}$ are assumed to be non-trivial for the mechanism to work, though they are allowed to be reducible and may also contain trivial representations. We consider a symmetry such that the "action" S remains invariant,

$$S(\phi^{(g)}, Q^{(g)}) = S(\phi, Q), \tag{23}$$

and the group elements have determinant 1 such that

$$d\phi^{(g)} = d\phi, \tag{24}$$

which implies that

$$\Psi(Q^{(g)}) = \Psi(Q). \tag{25}$$

Here, it is also implicitly assumed that the integration contour $\mathcal{C}$ is invariant under the group action. However, this is not a general requirement, because, for instance, if the integral (21) is a holomorphic one, as in the case of Eq. (17), $\mathcal{C}$ is allowed to be transformed up to continuous deformations due to the Cauchy theorem.

One can make a good estimate of the preferred configurations of Q by considering the critical points ϕ^σ of the action:

$$\left.\frac{\partial S}{\partial \phi_a}\right|_{\phi=\phi^\sigma} = 0. \tag{26}$$

Summing up all the contributions of such critical points for the approximation of the full integral is called the stationary phase approximation.[15] Here, we want to use it to qualitatively predict the most important configurations by analyzing these critical points. Usually if there exist several critical points, the contributions of the critical points will have uncorrelated phases and will cancel each other out so that the sum will generally be small. However, in some cases it is possible to get a large sum, i.e., if we take a certain configuration Q_H that is invariant under a subgroup $H \subset G$. In this case,

[15] This terminology is for real S. The analogous method for complex cases is given by taking the main orders [28] in the Picard–Lefschetz theory [29].

because of the invariance of Eq. (23), the critical points form invariant sets with the same phase along the trajectories of the group action $h \in H$:

$$S(\phi^\sigma, Q_H) = S(\phi^{\sigma,(h)}, Q_H^{(h)}) = S(R(h)_a{}^b \phi_b^\sigma, Q_H). \tag{27}$$

Because the phase is constant, all the critical points contained in such an invariant set contribute coherently to Ψ.[16] If a critical point ϕ^σ is contained in the trivial part of the representation R, the invariant set contains only one element, and the critical point will be isolated in most cases. On the other hand, if the group action generates a non-trivial set of critical points (a continuous set if H is a continuous group), these critical points will give larger contributions than the isolated cases.

Generally speaking, this mechanism would prefer a larger representation space of H in the space of ϕ for larger amplification of Ψ. On the other hand, it seems rather difficult to determine whether higher-dimensional symmetries are preferred or not. A higher-dimensional symmetry will in general form a higher-dimensional subspace of the representation in the space of ϕ, and therefore the amplification for one particular Q_H will become larger. However, higher symmetries will require more conditions on Q_H, and the net probability of getting higher-dimensional symmetries can become smaller. Therefore, it seems a non-trivial question what kinds of symmetric configurations have the largest contributions in the end.

In the previous paper a certain toy model was analyzed, which is very similar to the current model of interest, Eq. (17), being obtained by setting $\tilde{\phi} = 1$ in Eq. (17):

$$\Psi(P) = \int d\phi \; e^{i(\phi^2 + P\phi^3)}. \tag{28}$$

This model was found to indeed support this highlighting mechanism of symmetric configurations.

4. Highlighted symmetries in the canonical tensor model

In this section, we first analyze the critical points in the action of the integral expression of the wave function (17) to obtain potential peaks expected from the highlighting mechanism of symmetries discussed in Sect. 3. We find that $\lambda > 0$ is required for the existence of interesting critical points. We give a numerical method for the explicit evaluation of the wave function (17). The regularization and its vanishing limit by means of a contour deformation are discussed in some detail. Finally we show that, for a few concrete examples, we indeed find strong peaks at symmetric configurations in accordance with the highlighting mechanism.

4.1. Critical points

The "action" of the wave function given in Eq. (17),

$$S(P, \phi, \tilde{\phi}) = P\phi^3 + \phi^2\tilde{\phi} - \frac{4}{27\lambda}\tilde{\phi}^3, \tag{29}$$

is invariant under the following $O(N)$ transformations:

$$\begin{aligned} P_{abc} &\to L_{aa'} L_{bb'} L_{cc'} P_{a'b'c'}, \\ \phi_a &\to L_{aa'} \phi_{a'}, \end{aligned} \tag{30}$$

[16] Since the whole system of ϕ is invariant under H for $Q = Q_H$, the coherence is an exact phenomenon beyond the stationary phase approximation.

where L denotes the fundamental $O(N)$ matrices. The existence of such an underlying symmetry is one of the conditions for the mechanism in Sect. 3 to work, and the present model may have the highlighting phenomena for the symmetric configurations.

To start, let us analyze the critical points of Eq. (29). From Eq. (26) one finds the equations to be given by

$$\begin{aligned} 3(P\phi^{\sigma\,2})_a + 2\phi^\sigma_a \tilde{\phi}^\sigma &= 0, \\ \phi^{\sigma\,2} - \frac{4}{9\lambda}\tilde{\phi}^{\sigma\,2} &= 0, \end{aligned} \tag{31}$$

where ϕ^σ and $\tilde{\phi}^\sigma$ denote the critical points of ϕ and $\tilde{\phi}$ respectively, labeled by σ. If $\tilde{\phi}^\sigma \neq 0$ we can rewrite the equations with the rescaled variable $\varphi^\sigma = \phi^\sigma/\tilde{\phi}^\sigma$, and obtain

$$\begin{aligned} 3(P\varphi^{\sigma\,2})_a + 2\varphi^\sigma_a &= 0, \\ \varphi^{\sigma\,2} - \frac{4}{9\lambda} &= 0. \end{aligned} \tag{32}$$

The first equation is nothing but the critical point equation of the previous model (28). Therefore, one can expect that the symmetry highlighting phenomena will similarly occur in the present model as in the previous one (28) (as analyzed in Ref. [23]). Here the only difference comes from the second equation, which restricts the size of φ^σ to be a constant. Since, from the first equation, the size of φ^σ is inversely proportional to that of P, the second equation actually restricts the size of P. This implies that, unlike the previous model (28), the values of P for which there exist critical points are restricted by an additional condition. This can be obtained by eliminating $\tilde{\phi}^\sigma$ from Eq. (31):

$$\lambda = \frac{(P\phi^{\sigma\,3})^2}{(\phi^{\sigma\,2})^3}. \tag{33}$$

This is indeed independent of the overall scale of ϕ^σ, giving a restriction on the size of P. This relation is consistent only for $\lambda > 0$. For $\lambda < 0$, from Eq. (31), there are no other critical points than the trivial one $\phi = \tilde{\phi} = 0$, and we cannot expect the wave function to have interesting structures.[17] Because $\lambda = 0$ has already been discarded in Sect. 2, we will exclusively consider the $\lambda > 0$ case in this paper.

Following the argument of Sect. 3, we want to consider the subgroups of the full symmetry group $O(N)$ under which the configuration P_{abc} itself is invariant. These configurations are expected to be more relevant than the configurations without such symmetric properties. The primary possibilities of symmetries are $O(n)$ $(n < N)$, $O(n) \times O(m)$ $(n+m < N)$, and so on. Other interesting possibilities are the Lie groups with real orthogonal representations, which can be embedded into the $O(N)$ matrices of the underlying symmetry (30). To see whether these configurations are preferred, it is necessary to develop some tools to actually calculate the integral (17). This is highly non-trivial, and few things can be done analytically. But numerical tools will prove to be of value.

4.2. Evaluating the wave function

In this section, we reduce the $N+1$-dimensional integral of Eq. (17) to an N-dimensional compact integral. This is valid for generic P, and hence is very useful to analyze the behavior for generic P.

[17] As a check of this statement, we have computed the wave function for some cases with $\lambda < 0$ by the method explained in the later sections, and have actually observed its monotonous nature.

Though the expression is in principle exact, numerical evaluation might be slow and inaccurate in general due to the remaining numerical integration over N variables.

Taking advantage of the fact that $S(P,\phi,\tilde{\phi})$ in Eq. (29) is a homogeneous cubic function of ϕ and $\tilde{\phi}$, we can do a coordinate transformation to hyperspherical coordinates. For notational simplicity, we introduce $\tilde{P}$ as the tensor expressing $\tilde{P}_{abc}\phi_a\phi_b\phi_c = S(P,\phi,\tilde{\phi})$ in Eq. (29), where we regard $\phi_{N+1} = \tilde{\phi}$. With hyperspherical coordinates, ϕ can be decomposed into an angular and a radial part as $\phi_a = \phi_{\Omega\,a} r$, where Ω denotes a set of angular coordinates, and ϕ_Ω is a unit vector oriented in the direction described by Ω. By this change of variables, we obtain

$$\Psi(P) = \int_{S^N} d\Omega \int_0^\infty dr\, r^N e^{i(\tilde{P}\phi_\Omega^3)r^3 - \epsilon\, r^3}, \tag{34}$$

where we have introduced the $\epsilon\, r^3$ term with a positive small ϵ as a regulator. The r integration can now be done by using $\int_0^\infty dr\, r^N e^{-(\epsilon - ia)r^3} = \frac{1}{3}\Gamma(\frac{N+1}{3})(\epsilon - ia)^{-\frac{N+1}{3}}$:

$$\Psi(P) = \frac{1}{3}\,\Gamma\left(\frac{N+1}{3}\right)\int_{S^N} d\Omega\, \frac{1}{(\epsilon - i\tilde{P}\phi_\Omega^3)^{\frac{N+1}{3}}}. \tag{35}$$

Here the branch cut of the fractional power is assumed to be taken on the negative real axis. This will always be assumed for other fractional powers and logarithmic functions appearing in this paper without further notice. Now the problem of computing the wave function is reduced to a compact N-dimensional integration. However, the $\epsilon \to 0^+$ limit has an apparent difficulty of diverging on the points Ω satisfying $\tilde{P}\phi_\Omega^3 = 0$. For generic $\tilde{P}$, this divergence is not a real property of the wave function, because the singular points can be circumvented by considering appropriate deformation of the integration contour away from the real plane as shown in Fig. 1. Such deformation is allowed because of the Cauchy's integral theorem. For the numerical computation, one can systematically perform this deformation by doing a change of variables, which adds some imaginary values to the spherical coordinates:

$$\Omega_j' = \Omega_j + i\Delta\frac{\partial(\tilde{P}\phi_\Omega^3)}{\partial\Omega_j}, \tag{36}$$

where Δ is a small positive number, Ω_j $(j = 1, 2, \ldots, N)$ are the spherical coordinates taking real values, and Ω_j' are the deformed coordinates that are generally complex. If Δ is positive and small

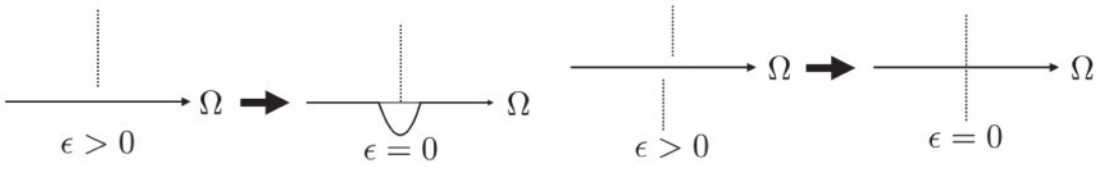

Fig. 1. An illustration of the deformation of the integration contour. The integration contours are described by the thick lines, and the branch cuts of the integrand by the dotted ones. On the left, for $\epsilon > 0$, the contour can be taken on a real line, and can safely be deformed without being singular in the $\epsilon \to 0^+$ limit. The deformation cannot be done if the integration contour is pinched by two branch cuts in the $\epsilon \to +0$ limit, as in the right figure.

enough, this deformation will deform the contour appropriately, because[18]

$$\tilde{P}\phi^3_{\Omega'} = \tilde{P}\phi^3_{\Omega} + i\sum_{j=1}^{N}\Delta\left(\frac{\partial(\tilde{P}\phi^3_{\Omega})}{\partial\Omega_j}\right)^2 + \mathcal{O}(\Delta^2), \tag{37}$$

and the second term on the right-hand side effectively add a positive contribution to ϵ in the denominator of Eq. (35). This will enable one to smoothly take the $\epsilon \to 0^+$ limit. With this change of variables, Eq. (34) has now been transformed to

$$\Psi(P) = \frac{1}{3}\,\Gamma\left(\frac{N+1}{3}\right)\int_{S^N} d\Omega \left|\frac{\partial\Omega'}{\partial\Omega}\right| \frac{1}{(-i\tilde{P}\phi^3_{\Omega'})^{\frac{N+1}{3}}}, \tag{38}$$

which does not contain ϵ anymore.

As can easily be seen in Eq. (37), the aforementioned method of deforming the contour does not work properly on the Ω for which $\tilde{P}\phi^3_{\Omega} = 0$ and $\partial(\tilde{P}\phi^3_{\Omega})/\partial\Omega_i = 0\ \forall i$. Since the former can be regarded as the derivative of $\tilde{P}\phi^3$ with respect to r and the latter with respect to the angular variables, the condition is nothing but $\partial(\tilde{P}\phi^3)/\partial\phi_a = 0\,\forall a$, namely the condition (26) for a critical point of $\tilde{P}\phi^3$. As explained in Sect. 4.1, non-trivial critical points exist[19] only for special values of $\tilde{P}$, namely those satisfying Eq. (33). In other words, there is a correspondence between the singularities of the wave function and the condition (33) derived from the existence of critical points. Thus, the expression (38) is non-singular and valid for generic $\tilde{P}$, but singular for special $\tilde{P}$ allowing the existence of critical points. A typical example of a singular case is illustrated in the right figure of Fig. 1, where the deformation cannot be done because of a pinch by two branch cuts, reflecting the singularity of the wave function on this point in the $\epsilon \to +0$ limit. As used above, in this paper, we often use "generic" and "special" to describe the non-singular and singular cases of P (and $\tilde{P}$), respectively.

A consistency check of the final expression of the wave function (38) can be done by looking at the dependence of the value on the deformation parameter Δ. The wave function should not depend on Δ due to the Cauchy theorem, unless the contour crosses some cuts or singularities by the deformation. A more thorough consistency check is to directly see whether the constraint equations (15) and (16) are satisfied by Eq. (38). We have obtained some fairly good numerical results supporting the validity of Eq. (38). The details are given in the last part of Appendix A.

The expression (38) has the advantage that it is in principle valid for generic P and any N. It is certainly useful to study the wave function at general values of P for small N. However, it still contains the N-variable integration, so for larger N the numerical integration takes much time and may contain large numerical errors. Therefore it is not really useful for studying the large-N behavior of the wave function. For that reason, in Sect. 5, we consider a subspace of P, where one can analytically perform all the integrations but one, which is numerically evaluated. This subspace is still large enough to contain both the symmetric and non-symmetric configurations, and is therefore useful for our purpose to see the highlighting phenomena of symmetric configurations.

4.3. An example

To give a concrete example of the application of the mechanism explained in Sect. 3 we consider $N = 3$. The case of $N = 3$ has just one Lie subgroup that can be highlighted by the mechanism:

[18] Here, we implicitly take the expression of $\tilde{P}\phi^3_{\Omega}$ as a holomorphic function of Ω.
[19] Note that the trivial critical point $\phi = 0$ plays no role in Eq. (38).

$O(2) \subset O(3)$. A tensor P_{abc} invariant under an $SO(2)$ transformation can be obtained by solving

$$T_{aa'}P_{a'bc} + T_{bb'}P_{ab'c} + T_{cc'}P_{abc'} = 0, \tag{39}$$

where T_{ab} is the generator of the $SO(2)$ transformation. There always exists an $O(3)$ transformation to put this generator in the following form:

$$T = \begin{bmatrix} 0 & 1 & 0 \\ -1 & 0 & 0 \\ 0 & 0 & 0 \end{bmatrix}. \tag{40}$$

Equation (39) can then be found to be solved by

$$\begin{aligned} P_{113} &= P_{223} = \frac{x}{3}, \\ P_{333} &= y, \end{aligned} \tag{41}$$

where the other components (up to permutations) are zero. The action of Eq. (29) for this configuration is given by

$$S = x(\phi_1^2 + \phi_2^2)\phi_3 + y\phi_3^3 + (\phi_1^2 + \phi_2^2 + \phi_3^2)\tilde{\phi} - \frac{4}{27\lambda}\tilde{\phi}^3, \tag{42}$$

which is $O(2)$ invariant. The (real) critical points (26) of the action are given by

$$\phi_1 = \phi_2 = \phi_3 = \tilde{\phi} = 0, \tag{43}$$

$$\phi_1 = \phi_2 = 0,\ \phi_3 = -\frac{2}{3y}\tilde{\phi}, \qquad \text{for } \lambda = y^2, \tag{44}$$

$$\phi_1^2 + \phi_2^2 = R^2\tilde{\phi}^2,\ \phi_3 = -\frac{1}{x}\tilde{\phi}, \qquad \text{for } \lambda = \frac{4x^3}{27(x-y)}, \tag{45}$$

where $R^2 = \frac{2x-3y}{x^3} > 0$. The result is really similar to the one found for the previous model (28) [23], with the major difference coming from Eq. (33): Each critical point, except the trivial one, has a restriction on the configuration variables, x and y, which is shown as the second equation in each line.

Figure 2 displays clearly the symmetry highlighting phenomenon of the present model consistent with the discussions in Sect. 3: The wave function has strong peaks along the trajectory represented by the second equation of Eq. (45) with $R^2 > 0$, while there are small peaks along the second equation of Eq. (44). As discussed there, one can see that the continuous critical points, namely Eq. (45), contribute much more than the isolated one (44). One can also observe that the peaks exist along the classical paths of the CTM, as shown in the right figure, where the classical equation of motion is given by

$$\frac{dP_{abc}}{dt} = \{\mathcal{H}_3, P_{abc}\} \tag{46}$$

with an auxiliary parameter t. Here, the Hamiltonian vector flow of $\mathcal{H}_3$ has directions within the x, y plane, since this preserves the $O(2)$ symmetry. Thus, the strong peaks can be regarded as representing a particular classical path, giving an explicit example of the emergence of classicality in the quantum CTM.

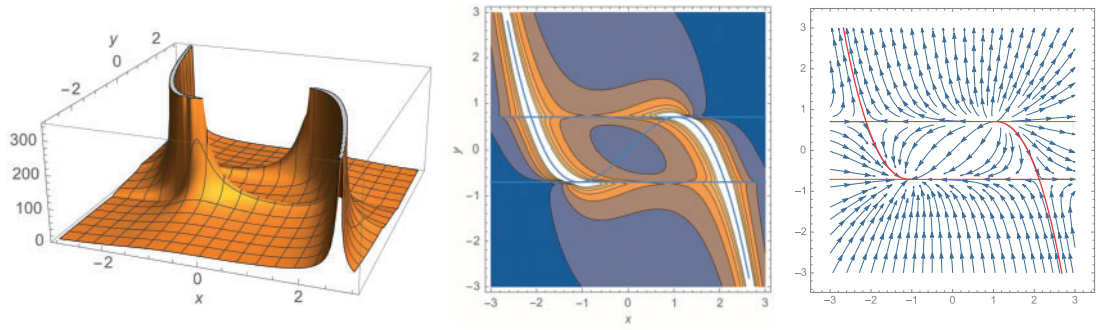

Fig. 2. Left: A 3D plot of the absolute value of the wave function (38) for Eq. (42) with $\lambda = 0.5$, drawn on the (x, y) parameter plane. The values over 300 have been chopped. Middle: The same function as the left, but as a contour plot. The blue solid curve and the straight lines respectively represent the restrictions $y = x - \frac{4}{27\lambda}x^3$ in Eq. (45) and $y^2 = \lambda$ in Eq. (44). The configurations along Eq. (45) with $R^2 > 0$ are strongly peaked. The smaller effects along Eq. (44) are also visible. Right: The arrows represent the Hamiltonian vector flow of $\mathcal{H}_3$ of the classical CTM.

One can add other terms to the action of Eq. (42) to disrupt the symmetry. From the discussion in Sect. 3 one would expect that any such terms will make the wave function smaller. For this example we will focus on one term specifically; the others can also be calculated well. The term we add here is given by

$$\delta S = z\phi_1\phi_3^2, \tag{47}$$

where z is a parameter corresponding to $P_{133} = z/3$. One can reduce the integral with this term to a single compact integral:

$$\begin{aligned}
\Psi(P) &= \int d\phi d\tilde{\phi}\, e^{i(\phi_1^2(x\phi_3+\tilde{\phi})+\phi_2^2(x\phi_3+\tilde{\phi})+z\phi_1\phi_3^2+y\phi_3^3+\phi_3^2\tilde{\phi}-\frac{4}{27\lambda}\tilde{\phi}^3)} \\
&= \int d\phi_3 d\tilde{\phi} \frac{i\pi}{x\phi_3+\tilde{\phi}} e^{i(y\phi_3^3+\phi_3^2\tilde{\phi}-\frac{4}{27\lambda}\tilde{\phi}^3-\frac{z^2\phi_3^4}{4(x\phi_3+\tilde{\phi})})} \\
&= \int dr d\theta \frac{i\pi}{x\cos\theta+\sin\theta} e^{i(y\cos^3\theta+\cos^2\theta\sin\theta-\frac{4}{27\lambda}\tilde{\phi}^3-\frac{z^2\cos^4\theta}{4(x\cos\theta+\sin\theta)})r^3} \\
&= i\pi\Gamma(4/3)\int d\theta \frac{\left(-i\left(y\cos^3\theta+\cos^2\theta\sin\theta-\frac{4}{27\lambda}\sin^3\theta-\frac{z^2\cos^4(\theta)}{4(x\cos\theta+\sin\theta)}\right)\right)^{-1/3}}{x\cos\theta+\sin\theta},
\end{aligned} \tag{48}$$

where a similar deformation of the integration contour as in Eq. (38) is implicitly taken.

The integral (48) can be evaluated numerically, one example of which can be found in Fig. 3. One can see that indeed the wave function has a peak for $z = 0$, so the symmetric configuration is preferred.

5. Simplified calculable model

In this section we treat a simplified model by restricting P to a subspace. The motivation for this is to reduce the number of numerical integrations needed for the evaluation of the wave function, as the numerical integrations over multiple variables take much time and are not always reliable due to numerical errors. In this subspace, the integrations in Eq. (17) can be done analytically except for

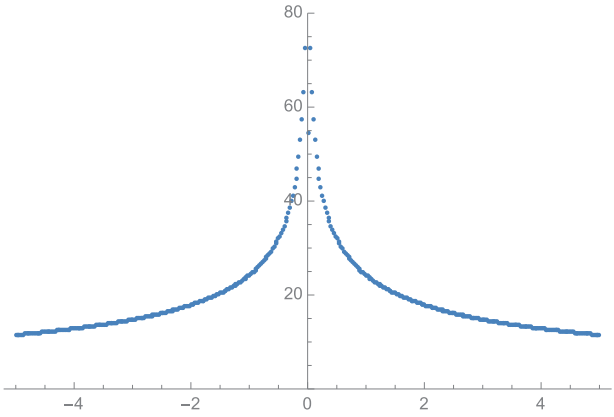

Fig. 3. The evaluation of the integral (48) with $x = 3$, $y = x - \frac{4}{27\lambda}x^3$, $\lambda = 1$. This is plotted against z, and the symmetric configuration $z = 0$ is clearly preferred.

one integration, which can be numerically evaluated much more easily. The restriction does not spoil our main purpose: The subspace is large enough to observe the symmetry highlighting phenomenon in the CTM, though it is not enough to predict the most preferred symmetric configuration in the full configuration space. Because of the single remaining numerical integration, the model can be used to numerically study the behavior of the wave function for large N, which is virtually impossible by the method described in Sect. 4.2.

The model that we consider is given by

$$\Psi(x,y) = \int d\phi d\tilde{\phi}\, e^{iS(\phi,\tilde{\phi},x,y)}, \tag{49}$$

where

$$S(\phi,\tilde{\phi},x,y) = \sum_{i=1}^{N-1} x_i\phi_i^2\phi_N + y\phi_N^3 + \phi^2\tilde{\phi} - k\tilde{\phi}^3 \tag{50}$$

with $k = \frac{4}{27\lambda}$. When x_i are all equivalent, the action is invariant under an $O(N-1)$ symmetry. When all values of x_i are different, the $O(N-1)$ symmetry is broken to $O(1)^{N-1} \cong Z_2^{N-1}$. We also have the intermediate cases with $\bigotimes_{i=1}^{k} O(n_i)$ with $n_1 + \ldots + n_k = N-1$ by considering some sets of equivalent x_i as the following illustrative example:

$$(x_i) = (\overbrace{x_1, x_1, x_1}^{O(3)}, \overbrace{x_2, x_2}^{O(2)}, \overbrace{x_3}^{O(1)}, \overbrace{x_4, x_4}^{O(2)}, \ldots). \tag{51}$$

This fact makes this model interesting for the study of the symmetry highlighting phenomena, though the subspace is really small compared to the whole space of P.

One can analytically integrate over ϕ_i $(i = 1, 2, \ldots, N-1)$ in Eq. (49), because these are just Gaussian integrations. After this exercise there remain two integrations, over ϕ_N and $\tilde{\phi}$, and one of them can be done in a similar manner to the radial integration in Eq. (34). By doing this integration we obtain

$$\Psi = 2\pi^{\frac{N-1}{2}} \mathrm{Re}\,[A_+], \tag{52}$$

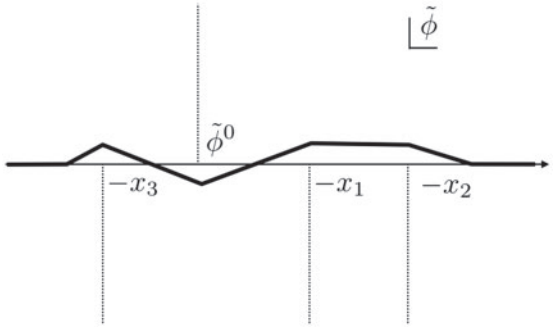

Fig. 4. An example of the integration contour $\mathcal{C}$ of $\tilde{\phi}$. The dotted lines are the branch cuts of the integrand. $\tilde{\phi}^0$ denotes a real solution to $h(\tilde{\phi}) = 0$. The example is shown for $h'(\tilde{\phi}^0) < 0$.

where A_+ is given by

$$A_+ = \frac{1}{3}\Gamma\left(\frac{5-N}{6}\right)\int_{\mathcal{C}} d\tilde{\phi}\prod_{j=1}^{N-1}\frac{1}{\sqrt{-i(x_j+\tilde{\phi})}}\left(-ih(\tilde{\phi})\right)^{\frac{N-5}{6}}, \tag{53}$$

with $h(\tilde{\phi}) = \tilde{\phi} + y - k\,\tilde{\phi}^3$ if $(N-5)/6$ is not an integer, or Eq. (C12) if $(N-5)/6$ is an integer. The detailed derivation is given in Appendix C. The integration contour $\mathcal{C}$ should be taken so as to avoid the branch cuts of the integrand as illustrated in Fig. 4. This is determined by the vanishing limit of the regularization, as explained in Appendix C. Since there remains only one integration, the numerical evaluation is relatively easy, even for a large N.

From expression (53) (or (C12)), one can easily see the symmetry highlighting phenomena in this simplified case. As in the right figure of Fig. 1, the wave function will have singularities if the integration contour is pinched by some branch cuts. In the example of Fig. 4, this occurs if some of $-x_i$ coincides with $\tilde{\phi}^0$, and the number, say n, of $-x_i$ that accumulates at $\tilde{\phi}^0$ will determine the highlighted symmetry to be $O(n)$.

In general, as explained in Appendix C, the branch cuts of the square roots of the integrand extend in the negative imaginary direction, while those of $(-ih(\tilde{\phi}))^{(N-5)/6}$ (or $\log(-ih(\tilde{\phi}))$ for integer $(N-5)/6$ and similarly below) extends from the point where $h(\tilde{\phi}) = 0$ on the real axis in the positive imaginary direction if $h'(\tilde{\phi}) < 0$ at the point and the negative imaginary direction if $h'(\tilde{\phi}) > 0$. Due to the simple cubic form of $h(\tilde{\phi})$ in $\tilde{\phi}$, there only exist two major cases for the branch cuts of $(-ih(\tilde{\phi}))^{(N-5)/6}$. These are (i) $y^2 > \lambda$: One branch cut extends in the positive imaginary direction, or (ii) $y^2 < \lambda$: Two branch cuts extend in the positive imaginary direction, and one in between extends in the negative imaginary direction. Since the pinching occurs only when the positive and negative branch cuts meet, we have the following three major kinds of singularities of the wave function:

- At $y^2 = \lambda$, two of the branch cuts of $(-ih(\tilde{\phi}))^{(N-5)/6}$, one extending in the negative imaginary direction and the other in the positive, pinch the contour.
- At $y^2 > \lambda$, $O(n)$ symmetric configurations are highlighted by the accumulation of n of $-x_i$ to the one branch point of $(-ih(\tilde{\phi}))^{(N-5)/6}$.
- At $y^2 < \lambda$, $O(n_1)\times O(n_2)$ symmetric configurations are highlighted by the similar accumulation above to the two branch points of $(-ih(\tilde{\phi}))^{(N-5)/6}$ whose branch cuts extend in the positive imaginary directions.

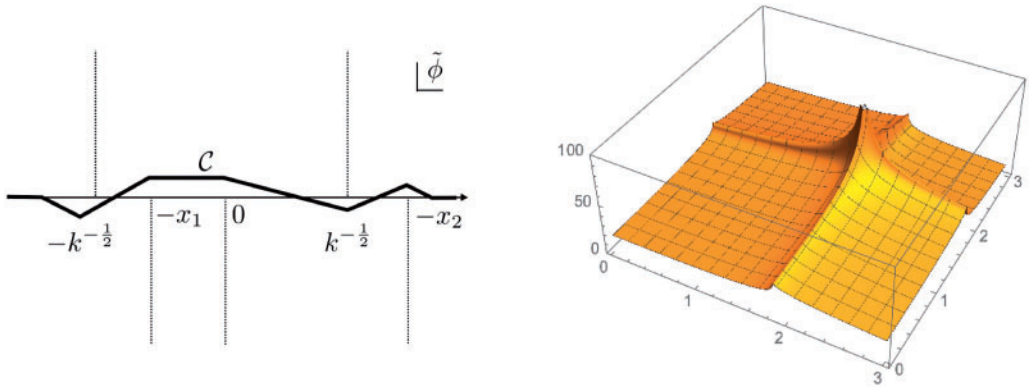

Fig. 5. Left: The branch cuts of the integrand and the integration contour $\mathcal{C}$ for Eq. (54). Right: A 3D plot of the wave function plotted on the (x_1, x_2) plane for $N = 3$, $y = 0$, and $\lambda = 0.5$. There are small peaks corresponding to the case that one of the x_i is on $k^{-1/2}$, and a large peak corresponding to the highlighting of an $O(2)$ symmetry at $x_1 = x_2 = k^{-1/2}$. The values over 100 have been chopped.

The first one corresponds to the small peak described in Eq. (44) for $N = 3$, and the second and third to that in Eq. (45), where only an accumulation to one branch point is considered in Eq. (45) due to $x_1 = x_2 = x$. One important thing to notice is that, while the action (50) can have various $\bigotimes_{i=1}^{k} O(n_i)$ symmetries, the actual highlighted symmetries are limited to $O(n)$ or $O(n_1) \times O(n_2)$.

As a concrete example, let us consider the simple case with $N = 3, y = 0$ of Eq. (50). In this case, Eq. (53) has the form

$$A_+^{N=3,y=0} \propto \int_{\mathcal{C}} d\tilde{\phi}\ (-i(x_1+\tilde{\phi}))^{-\frac{1}{2}}(-i(x_2+\tilde{\phi}))^{-\frac{1}{2}}(-i\tilde{\phi}(1+\sqrt{k}\tilde{\phi})(1-\sqrt{k}\tilde{\phi}))^{-\frac{1}{3}}. \tag{54}$$

The branch cuts of the integrand and the integration contour $\mathcal{C}$ are illustrated in the left figure of Fig. 5. There are three branch points coming from $h(\tilde{\phi}) = 0$, i.e., $\tilde{\phi} = 0, \pm k^{-1/2}$, and singular behavior is expected for $x_i = \pm k^{-1/2}$, but not for $x_i = 0$ because of the absence of a pinch. If only one of x_i is at $\pm k^{-1/2}$, the singularity of the integrand is not strong enough for the integral to diverge, but there will be a rapid change of the value when x_i passes over $\pm k^{-1/2}$, because the integration contour gets substantially changed. If $x_1 = x_2 = \pm k^{-1/2}$, the integral diverges, and the wave function has a strong peak there.[20] This indeed corresponds to an $O(2)$ symmetric configuration, and is interpreted as an occurrence of the symmetry highlighting phenomenon (see the right figure of Fig. 5).

As mentioned at the beginning of this section, this simplified setting gives a relatively simple way to do some analysis on the large-N behavior and to explore some of the possible symmetric configurations. To do the analysis of the first problem we will introduce a parameterization of just one parameter z, which breaks the $O(N-1)$ symmetry completely to $O(1)^{N-1}$, given by

$$x_i(z) = x_0 + z\left(\frac{i}{N} - \frac{1}{2}\right). \tag{55}$$

This parameterization is chosen such that x_i $(i = 1, 2, \ldots, N-1)$ are distributed evenly in the region,

$$x_i(z) \in \left(x_0 - \frac{z}{2}, x_0 + \frac{z}{2}\right) \tag{56}$$

[20] In this paper, we will not discuss whether this divergence is square integrable over P or not, because, for that, we need the understanding of the behavior in the full parameter space of P, which is out of our present reach.

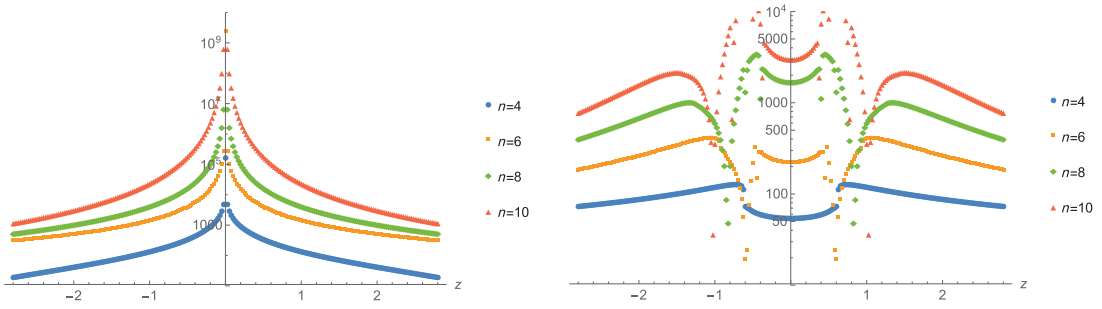

Fig. 6. Left: The absolute value of the wave function plotted against z for $N = \{4, 6, 8, 10\}$ with $x_0 = 2$, $y = x_0 - kx_0^3$, $k = 4/27$. Right: The same for $x_0 = 2$, $y = x_0 - kx_0^3 + 0.1$, $k = 4/27$. It is clear that even a small number of α changes the overall structure. There even exist locations where the wave function changes its sign. These appear as sharp valleys in the plot of the absolute value. Comparing the two figures, one can see that the peak for $\alpha = 0$ is much stronger.

with a center at x_0. Once one understands the behavior of this for large N, one might be able to get a hint about the $N \to \infty$ limit for the simplified model (50). However, this parameterization reduces the configuration space even further, making the predictions somewhat modest.

For y, we shall choose a value of

$$y = x_0 - kx_0^3 + \alpha, \tag{57}$$

where α is the parameter that we will change. When $\alpha = 0$, the relevant branch point of $(-ih(\tilde{\phi}))^{(N-5)/6}$, written in $x = -\tilde{\phi}$, is located at the center $x = x_0$ of the region (56). Therefore, if we take $|z|$ smaller, x_i accumulate toward the branch point and the configuration approaches an $O(N-1)$ symmetric one. Indeed, as seen in the left figure of Fig. 6, there is a strong peak at $z = 0$, as expected from the highlighting mechanism. The peak is enhanced for larger N.

If we take a non-zero value for α, $z = 0$ is no longer the case in which the accumulation of x_i toward the branch point occurs. In fact, the region (56) contains the branch point only for $|z| > z_{\min}$ with a positive value of $z_{\min}$. The minimum $z_{\min}$ can be obtained by solving the condition for one of the endpoints[21] of the region (56) to coincide with the branch point, e.g. $y = x_0 + z/2 - k(x_0 + z/2)^3$ with Eq. (57) for $x_0, z > 0$. Indeed, as can be seen in the right figure of Fig. 6, the peaks are located away from $z = 0$. What occurs around the peaks is that $x_i(z)$ pass over the the branch point one by one in the course of changing the value of z. The highlighted symmetry is just $O(1)$ for each passing over. The wave function has some rich structures, seemingly reflecting the one-by-one passing over. The amplitude of the wave function is enhanced for larger N, but is substantially smaller than the $O(N-1)$ case in the left figure. Note also that for non-zero α, even though the point $z = 0$ still corresponds to an $O(N-1)$ symmetric configuration, this is not a large peak, since it misses the condition (33). Rather, the condition is satisfied for a highlighted $O(1)$ symmetry, when one of the $x_i(z)$ passes over the branch point.

For the large-N limit one can also use this setup and see if eventually this wave function will converge to something meaningful. While the case for $\alpha \sim 0$ seems to be rather simple, the situation for non-zero α seems to be much more complex. As explained above, the wave function as a function of z is made of a collection of $O(1)$ symmetric peaks, whose amount is $N-1$. Among them, the

[21] Here we ignore a small difference coming from the fact that the endpoints of the region (56) are not contained as x_i. For large N this is justified.

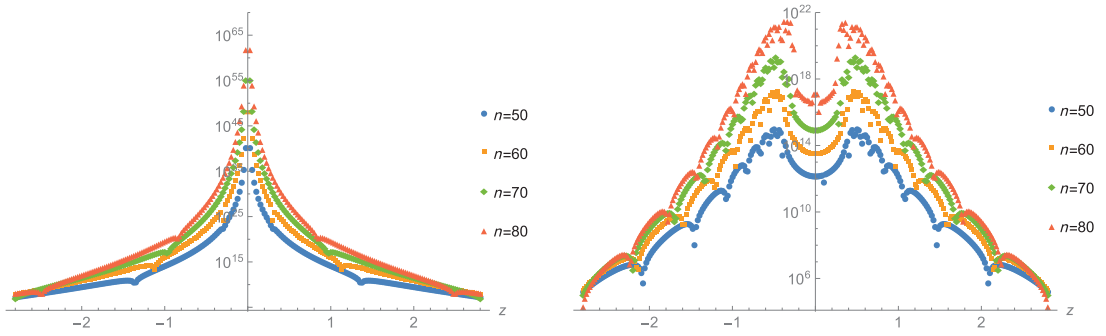

Fig. 7. Left: The absolute value of the wave function plotted against z for $N = \{50, 60, 70, 80\}$ with $x_0 = 2$, $y = x_0 - kx_0^3$, $k = 4/27$. Right: The same for $y = x_0 - kx_0^3 + 0.1$. The wave function for finite α has more structures and is not peaked around $z = 0$. The peak is much stronger for $\alpha = 0$.

peaks closer to $z = 0$ appear to become more and more important for larger N, which is due to the high density of peaks in this region. These things can be seen in Fig. 7.

Lastly we will investigate the behavior of the simplified model for other symmetries. As mentioned at Eq. (51), it is possible to find several subgroups in the configuration x_i. Let us consider the case symmetric under a product group, $O(n_1) \times O(n_2)$ with $n_1 + n_2 = N - 1$, having the following x_i:

$$(x_i) = (\overbrace{x_1, ..., x_1}^{n_1 \text{ times}}, \overbrace{x_2, ..., x_2}^{n_2 \text{ times}}) . \tag{58}$$

This is supposed to be the maximum possibility of the highlighted product group symmetry, because a product group with more than two $O(n_i)$ cannot be highlighted, as mentioned earlier in the analysis of the singularity of the wave function. For Eq. (58), one can derive the following two sets of continuous critical points in the same manner as deriving Eq. (45) of the previous example:

$$\begin{aligned} &\phi_1^2 + ... + \phi_{n_1}^2 = R_1^2 \tilde{\phi}^2, \ \ \phi_N = -\frac{1}{x_1}\tilde{\phi}, \text{ others} = 0, \\ &\phi_{n_1+1}^2 + ... + \phi_{N-1}^2 = R_2^2 \tilde{\phi}^2, \ \ \phi_N = -\frac{1}{x_2}\tilde{\phi}, \text{ others} = 0, \end{aligned} \tag{59}$$

where $R_i^2 = \frac{2x_i - 3y}{x_i^3}$. Each set of the continuous critical points exists only if the extra restriction $y = x_i - kx_i^3$ is satisfied as in the second equation of Eq. (45). There is another way to derive this restriction by using the singular structure of the branch cuts, not by using the stationary phase approximation: As mentioned earlier, the wave function has singularities when $h(-x_i) = 0$, and solving this equation will lead to the same restriction. Obviously we get the $O(N-1)$ symmetry by putting $x_1 = x_2$.

From Eq. (59) one would expect two things. First, it seems that the continuous critical points in Eq. (59) have smaller orbit spaces than $O(n_1 + n_2)$, making $O(n_1 + n_2)$ probably the stronger symmetry. Second, it is possible for the sets of continuous critical points to coexist, highlighting the $O(n_1) \times O(n_2)$ symmetry, if $y = x_1 - kx_1^3 = x_2 - kx_2^3$ is satisfied with distinct x_1 and x_2. These two contributions of the continuous critical points interfere with each other, and they may add up or cancel each other depending on particular cases. An example for $N = 7$ with $k = 4/27$ and $y = 0.5$ is given in Fig. 8, where we see the peaks of various patterns of symmetries.

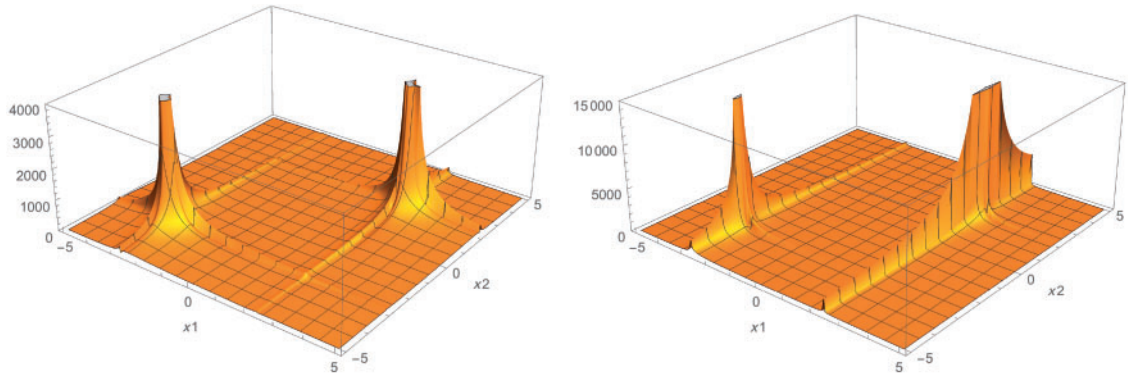

Fig. 8. Left: The wave function plotted against x_1, x_2 for a setup given by Eq. (58) for $O(3) \times O(3)$ symmetry. The largest peaks at $x_1 = x_2$ are of the $O(6)$ symmetry, and the shallow peaks extending from them the separate $O(3)$ symmetries. At the crossing points of the $O(3)$ peaks corresponding to $O(3) \times O(3)$, one can find a small additive effect. Right: The same for $O(4) \times O(2)$ symmetry. It can be seen that the $O(6)$ symmetry at $x_1 = x_2$ is most preferred, while the $O(4)$ peaks are much stronger then $O(2)$. At the point where $O(4) \times O(2)$ should occur, there should be an interference effect, but this cannot be easily seen because of the large difference of the strengths between $O(4)$ and $O(2)$. In both figures, the values over a certain level have been chopped.

6. Emergence of hidden spacetime symmetries

So far, we have only paid attention to the $O(N)$ symmetry, Eq. (6), which can be regarded as the space-like symmetry of the CTM in analogy with the ADM formalism. It would be reasonable to apply the highlighting mechanism to the $O(N)$ symmetry, since it is the kinematical symmetry of the CTM. However, while the symmetry is represented on the integration variable ϕ of the wave function (17), there exists the other integration variable $\tilde{\phi}$. Taking the mechanism more carefully, larger symmetries represented on both ϕ and $\tilde{\phi}$ have the possibility to be highlighted. Moreover, we also impose the Hamiltonian constraint $\mathcal{H}_a|\Psi\rangle = 0$, not only the kinematical one $\mathcal{J}_{ab}|\Psi\rangle = 0$. In this section, we will explicitly show that the above prospect for larger highlighted symmetries is indeed right in the example discussed in Sects. 4.3 and 5. Rather surprisingly, the hidden highlighted symmetries that we will find have spacetime signatures.

Let us first explain why we call these symmetries hidden. In Sect. 4.3, we solved the symmetry condition (39) for $N = 3$. There, the matrix T was assumed to be real and antisymmetric, and the $SO(2)$ symmetry turned out to be the unique possibility. This does not change, even if we consider T to be an arbitrary real matrix, and we still get only the $SO(2)$ symmetry as the unique possibility. It will turn out that not the fundamental dynamical variable of the theory, P, but rather the extended one (mentioned before in Sect. 4.2), $\tilde{P}$, will have a spacetime-like symmetry.

Following the line of thought from the first paragraph of this section, let us consider $\tilde{P}$ instead of P, where $\tilde{P}$ is the real symmetric rank-3 tensor parameterizing the whole action (42) including the part with $\tilde{\phi}$:

$$\begin{aligned}
&\tilde{P}_{113} = \tilde{P}_{223} = \frac{x}{3},\\
&\tilde{P}_{333} = y,\\
&\tilde{P}_{114} = \tilde{P}_{224} = \tilde{P}_{334} = \frac{1}{3},\\
&\tilde{P}_{444} = -k,
\end{aligned} \tag{60}$$

where $k = \frac{4}{27\lambda}$, we have regarded $\phi_4 = \tilde{\phi}$, and the other components up to permutations are zero. We now want to find the solutions to the symmetry condition

$$T_{aa'}\tilde{P}_{a'bc} + T_{bb'}\tilde{P}_{ab'c} + T_{cc'}\tilde{P}_{abc'} = 0 \tag{61}$$

with arbitrary 4-by-4 real matrices T (not restricted to be antisymmetric).

The number of the entries of T is 16, and it is easy to solve the condition by computer. For generic x, y, we again find only the $SO(2)$ matrix (40) as the solution. However, if we assume the second equation in Eq. (45), $y = x - k\,x^3$, for the continuous critical points, we obtain the following $T^{(2)}, T^{(3)}$ in addition to the $SO(2)$ generator (40) as solutions to Eq. (61):

$$T^{(2)}_{13} = T^{(3)}_{23} = 1,\ T^{(2)}_{14} = T^{(3)}_{24} = -x,\ T^{(2)}_{31} = T^{(3)}_{32} = -1 + \frac{3}{2}k\,x^2,\ T^{(2)}_{41} = T^{(3)}_{42} = -\frac{3}{2}k\,x, \tag{62}$$

where the other components are zero. One can check that they satisfy the following algebra:

$$\begin{aligned}
&[T^{(1)}, T^{(2)}] = -T^{(3)},\\
&[T^{(1)}, T^{(3)}] = T^{(2)},\\
&[T^{(2)}, T^{(3)}] = (3k\,x^2 - 1)\,T^{(1)},
\end{aligned} \tag{63}$$

where $T^{(1)}$ denotes the $SO(2)$ generator (40). As shown in Sect. 4.3, the strong peaks appear if $R^2 = \frac{2x-3y}{x^3} > 0$, which implies nothing but the positivity of the coefficient $3k\,x^2 - 1$ in the last line. Thus we have found an $SO(1,2)$ symmetry generated by $T^{(1,2,3)}$ as the highlighted symmetry on the strong peaks.

On the fixed points of the classical Hamiltonian vector flow the symmetry is enhanced even further. The flow is given by $\mathcal{H}_3$ (46), which is drawn in Fig. 2. There exist two kinds of fixed points, one at (i) $x = \pm 1/\sqrt{3k}$ and the other at (ii) $x = \pm 2/\sqrt{3k}$, on the curve $y = x - k\,x^3$. In each case, in addition to the above $T^{(1,2,3)}$ with the substitution of the values of x, there exists another symmetry transformation that solves Eq. (61):

$$\begin{aligned}
&\text{(i)}:\ T^{\mathrm{i}}_{11} = T^{\mathrm{i}}_{22} = \frac{1}{2},\ T^{\mathrm{i}}_{33} = 1,\ T^{\mathrm{i}}_{34} = \mp\frac{2}{\sqrt{3k}},\ T^{\mathrm{i}}_{43} = \mp\sqrt{3k},\\
&\text{(ii)}:\ T^{\mathrm{ii}}_{11} = T^{\mathrm{ii}}_{22} = 1,\ T^{\mathrm{ii}}_{33} = -1,\ T^{\mathrm{ii}}_{34} = \mp\frac{2}{\sqrt{3k}},\ T^{\mathrm{ii}}_{43} = \mp\sqrt{3k},
\end{aligned} \tag{64}$$

where the other components vanish. The algebras formed by them are respectively given by

$$\begin{aligned}
&\text{(i)}:\ [T^{(1)}, T^{\mathrm{i}}] = 0,\ [T^{(2)}, T^{\mathrm{i}}] = \frac{3}{2}T^{(2)},\ [T^{(3)}, T^{\mathrm{i}}] = \frac{3}{2}T^{(3)},\\
&\text{(ii)}:\ [T^{(1,2,3)}, T^{\mathrm{ii}}] = 0.
\end{aligned} \tag{65}$$

For general N with all $x_i = x$ in the simplified model discussed in Sect. 5, one can find a similar thing happening as above. The symmetry $SO(N-1)$ for general x, y is enhanced to the hidden $SO(1, N-1)$ symmetry at the strong peaks on $y = x - k\,x^3$, and there is an addition of another symmetry on each fixed point of the flow.

Presently we do not have a reliable physical interpretation of these highlighted hidden spacetime symmetries. These symmetries become apparent only after including the $\tilde{\phi}$ direction in the discussion of symmetries. This seems to suggest that this extra direction corresponds in some way to an implicit

time direction in the theory. This interpretation seems justified as the extra terms with $\tilde{\phi}$ are originally introduced to satisfy the Hamiltonian constraint. Moreover, the geometry of the critical points in Eq. (45) has the interesting structure of a circle that changes its radius in the $\tilde{\phi}$ direction. Though this looks like a time evolving system, the integration variables ϕ and $\tilde{\phi}$ have at this stage no physical interpretation. It is clear, however, that these emergent spacetime symmetries will play some important roles in the spacetime interpretation of the dynamics of the quantum CTM, which is yet to be explored.

7. Asymptotic behavior

The asymptotic behavior of the wave function (17) is also important to analyze. A sufficiently fast damping wave function at infinity would mean that the wave function is normalizable, at least up to singularities in the finite-P regime. Furthermore, the wave function turns out to have non-trivial asymptotic behavior worth investigating. In this section we will first show an easy example of the asymptotic behavior for a case with $N = 3$ showing some of the non-trivial behavior, then we will present a general scaling argument, which will be compared with some numerical results. The scaling argument seems to explain the asymptotic behavior in most cases, but will turn out not to cover all. In Appendix D, we show in part the normalizability of the wave function at infinity, based on the analysis of the asymptotic behavior discussed in this section.

The example was introduced in Sect. 4.3 and the resulting wave function is given in Eq. (48). Looking at the integrand, the asymptotic behavior with respect to x, y, and z naively seems to be

$$\begin{aligned}\Psi(x \to \infty) &\sim x^{-1},\\ \Psi(y \to \infty) &\sim y^{-1/3},\\ \Psi(z \to \infty) &\sim z^{-2/3}.\end{aligned} \tag{66}$$

However, the last asymptotic behavior is not right, and it is actually given by

$$\Psi(z \to \infty) \sim z^{-1/2}, \tag{67}$$

which can easily be checked by the numerical method given in the preceding sections. The reason for the difference from the naive expectation from the integrand is that the integrand is not uniformly convergent due to the pole. Therefore, in general, one has to carefully look into the integral to know the asymptotic behaviors in various infinite directions of the parameters. In the following section, we will give a scaling argument that would be applicable to most cases, including the above example. However, there do exist exceptional cases that cannot be understood simply by the scaling argument, and a more general method must be pursued in future study.

7.1. Scaling argument

In this subsection, we will describe a scaling argument that explains the asymptotic behavior of the wave function in most directions of large P. Let us consider the wave function (17),

$$\Psi(P) = \int_{\mathbb{R}^{N+1}} d\phi d\tilde{\phi}\, e^{i(P\phi^3+\phi^2\tilde{\phi}-k\tilde{\phi}^3)}, \tag{68}$$

where $k = \frac{4}{27\lambda}$ is assumed to be a positive constant. Throughout this subsection, it is implicitly assumed that the integration is appropriately defined by the prescription described in Sect. 4.2.

A natural rescaling of the integration variables would be given by

$$\phi_a \to |P|^{-\frac{1}{3}}\phi_a \ (a = 1, 2, \ldots, N), \tag{69}$$

where $|P| = \sqrt{P_{abc}P_{abc}}$. By the rescaling, the action in Eq. (68) is transformed as

$$P\phi^3 + \phi^2\tilde{\phi} - k\tilde{\phi}^3 \to |P|^{-1}P\phi^3 + |P|^{-\frac{2}{3}}\phi^2\tilde{\phi} - k\tilde{\phi}^3. \tag{70}$$

If one naively assumes that the middle term can be neglected in the large-P limit, Ψ will be estimated as

$$\Psi(P) \sim |P|^{-\frac{N}{3}} \int_{\mathbb{R}} d\tilde{\phi}\ e^{-ik\tilde{\phi}^3} \int_{\mathbb{R}^N} d\phi\ e^{i|P|^{-1}P\phi^3}. \tag{71}$$

The first integral takes a finite non-zero value, and the last integral does not depend on the overall scale of P. Therefore, when the last integral takes a finite non-zero value, the asymptotic behavior of Ψ, in which $|P|$ is taken infinitely large with constant $P_{abc}/|P|$, will be given by

$$\Psi(P) \sim \text{const.}\ |P|^{-\frac{N}{3}}, \tag{72}$$

where the overall factor is a function of $P_{abc}/|P|$. The crucial assumption here is that the last integral of Eq. (71) takes a finite non-zero value. For most values of P, this will be true, and the asymptotic behavior will be given by Eq. (72). However, there exist values of P for which this is not true, and there actually exist rich varieties of asymptotic behavior other than that.

A simple example with different asymptotic behavior can be obtained from the calculable model discussed in Sect. 5. By setting $y = 0$ in the model, we have

$$P\phi^3 = \sum_{i=1}^{N-1} x_i\phi_i^2\phi_N. \tag{73}$$

If a uniform rescaling $\phi_a \to |x|^{-\frac{1}{3}}\phi_a$ with $|x| = \sqrt{\sum_i x_i^2}$ for all the ϕ_a $(a = 1, 2, \ldots, N)$ is performed (as prescribed by Eq. (69)), and the limit $|x| \to \infty$ is taken, one obtains

$$P\phi^3 + \phi^2\tilde{\phi} - k\tilde{\phi}^3 \to \sum_{i=1}^{N-1} \frac{x_i}{|x|}\phi_i^2\phi_N - k\tilde{\phi}^3, \tag{74}$$

where the middle term has naively been assumed to be negligible in the limit. The right-hand side contains ϕ_N in a linear form, and this causes trouble. In fact, by performing the ϕ_N integration (and the $\tilde{\phi}$ integration) with the replacement (74), one obtains

$$\Psi \sim \text{const.}\ |x|^{-\frac{N}{3}} \int_{\mathbb{R}^{N-1}} \prod_{i=1}^{N-1} d\phi_i\ \delta\left(\sum_{i=1}^{N-1} \frac{x_i}{|x|}\phi_i^2\right). \tag{75}$$

Further integrations over ϕ_i $(i = 1, 2, \ldots, N-1)$ will be troublesome: the integral vanishes or diverges, depending on the signs of x_i, where the only finite case is $N = 3$ with $x_{1,2}$ having the same sign.

A correct way to deal with the above example is to consider a different rescaling than Eq. (69). To get a finite convergent result of the integration, the action has to take an appropriate form in the limit. In the present case, the $\phi_N^2\tilde{\phi}$ term contained in the middle term would be important in the limit,

because it would prevent ϕ_N from appearing only linearly, avoiding the problem above. So, rather than uniformly rescaling all the ϕ_a like Eq. (69), let us consider the following asymmetric rescaling:

$$\phi_i \to |x|^{-\frac{1}{2}}\phi_i \ (i = 1, 2, \ldots, N-1), \ \phi_N \to \phi_N. \tag{76}$$

By doing this rescaling and taking the limit $|x| \to \infty$, one obtains

$$P\phi^3 + \phi^2\tilde{\phi} - k\tilde{\phi}^3 \to \sum_{i=1}^{N-1} \frac{x_i}{|x|}\phi_i^2\phi_N + \phi_N^2\tilde{\phi} - k\tilde{\phi}^3, \tag{77}$$

where $\phi_N^2\tilde{\phi}$ indeed remains. Then, the expression

$$\Psi \sim |x|^{-\frac{N-1}{2}} \int_{\mathbb{R}^{N+1}} d\phi d\tilde{\phi} \ \exp\left[i\left(\sum_{i=1}^{N-1} \frac{x_i}{|x|}\phi_i^2\phi_N + \phi_N^2\tilde{\phi} - k\tilde{\phi}^3 \right)\right] \tag{78}$$

gives the asymptotic behavior $\Psi \sim$ const. $|x|^{-\frac{N-1}{2}}$, if the integral takes a finite non-vanishing value. This is actually the correct asymptotic behavior, if all the x_i have the same sign. In fact, the first line of Eq. (66) corresponds to the $N = 3$ case of Eq. (78). However, if the signs of x_i are mixed, the integral in Eq. (78) is divergent: the integral cannot be defined as a strictly convergent integration, as explained in the following. The ϕ_i integrations in Eq. (78) are Gaussian and diverge for $\phi_N = 0$. Therefore, to define the integral properly, one needs to deform the integration contour of ϕ_N in the vicinity $\phi_N \sim 0$. For the convergence of ϕ_i integration, the contour must be deformed as $\phi_N \to \phi_N + i\epsilon$ Sign(x_i) with a small positive ϵ in the vicinity $\phi_N \sim 0$. However, this can be done consistently for all ϕ_i, only if all x_i have the same sign.

In the case of mixed signs of x_i, one must consider another rescaling:

$$\phi_i \to \phi_i \ (i = 1, 2, \ldots, N-1), \ \phi_N \to \frac{1}{|x|}\phi_N. \tag{79}$$

Then, one obtains

$$\Psi \sim \frac{1}{|x|} \int_{\mathbb{R}^{N+1}} d\phi d\tilde{\phi} \ \exp\left[i\left(\sum_{i=1}^{N-1} \left(\frac{x_i}{|x|}\phi_N + \tilde{\phi} \right)\phi_i^2 - k\tilde{\phi}^3 \right)\right]. \tag{80}$$

In this case, the divergence of the ϕ_i integrations can be avoided by deforming the integration contour of ϕ_N in the manner mentioned above in the vicinity of $\frac{x_i}{|x|}\phi_N + \tilde{\phi} \sim 0$. In the present case, unless $\tilde{\phi} = 0$, the locations of ϕ_N satisfying $\frac{x_i}{|x|}\phi_N + \tilde{\phi} = 0$ are different for different x_i, and therefore there are no contradictions like the former case. Moreover, the point $\tilde{\phi} = 0$ can be circumvented by adding a small positive imaginary value to $\tilde{\phi}$ in the vicinity of $\tilde{\phi} \sim 0$ without ruining the convergence of the ϕ_i integrations. Here x_i must have mixed signs for the expression (80) to be useful, because otherwise the integral vanishes, which can be proved by deforming the integration contour of ϕ_N to the positive imaginary infinity. Thus the expression (80) shows that the asymptotic behavior is given by const. $/|x|$ for the mixed case. This turns out to be the correct one for $N \geq 4$, while $N = 3$ is exceptional, and will be discussed at the end of this subsection.

Let us summarize our scaling argument in general terms. We want to obtain the asymptotic behavior of Ψ for $|P| \to \infty$ with all $P_{abc}/|P|$ being fixed. Let us consider a rescaling,

$$\phi_a \to |P|^{-w_a}\phi_a \ (a = 1, 2, \ldots, N) \tag{81}$$

with some weights w_a. Then, Ψ is transformed to

$$\Psi = |P|^{-\sum_{a=1}^{N} w_a} \int_{\mathbb{R}^{N+1}} d\phi d\tilde{\phi}\ \exp\left[i\left(|P|^{-w_a-w_b-w_c} P_{abc}\phi_a\phi_b\phi_c + |P|^{-2w_a}\phi_a\phi_a\tilde{\phi} - k\tilde{\phi}^3\right)\right], \tag{82}$$

where the repeated indices are assumed to be summed over. This leads to the following two conditions: (i) The action in Eq. (82) has a finite limit in $|P| \to \infty$; (ii) The integral takes a finite non-zero value for the limiting action. Under these conditions, one obtains the asymptotic behavior

$$\Psi \sim \text{const.}\, |P|^{-\sum_{a=1}^{N} w_a}. \tag{83}$$

If one cannot find the set $\{w_a; a = 1, 2, \ldots, N\}$ that satisfies the two conditions above, the scaling argument cannot be applied. In fact, there exists such a counter example: The $N = 3$ case with $x_{1,2}$ having different signs. To see this, let us perform the ϕ_i integrations in Eq. (80). Then one obtains

$$\Psi \sim \frac{\text{const.}}{|x|} \int d\phi_N d\tilde{\phi} \prod_{i=1}^{N-1} \frac{1}{\sqrt{-i\left(\frac{x_i}{|x|}\phi_N + \tilde{\phi}\right)}} \exp\left(-ik\tilde{\phi}^3\right). \tag{84}$$

For $N = 3$, the integral over ϕ_N has a logarithmic divergence at infinity, and condition (ii) is violated. In fact, a numerical study shows that the asymptotic behavior of Ψ is given by $(c_1 + c_2 \log|x|)/|x|$ with constants $c_{1,2}$, which has the form of the naive expression $1/|x|$ accompanied by a logarithmic correction. Such a logarithmic correction cannot be treated by the present scaling argument. Therefore our scaling argument is not general enough to cover all the cases, though it seems applicable to most cases.

7.2. Examples

The general argument in the preceding subsection can now be used to explain the behavior of Eqs. (66) and (67). First, for the large x-behavior we let y and z be fixed. This gives the leading term of the action as

$$x(\phi_1^2 + \phi_2^2)\phi_3.$$

This corresponds to the first case of the example in the preceding subsection, namely $N = 3$ with $x_{1,2}$ having the same sign. Therefore, one obtains the behavior $1/x$, as can be extracted from Eq. (78), in agreement with Eq. (66).

Let us next consider the $y \to \infty$ limit with x, z being fixed. The leading term is given by

$$y\phi_3^3. \tag{85}$$

For this case, one is led to take $w_3 = 1/3$, because condition (i) requires $w_3 \geq 1/3$, but $w_3 > 1/3$ violates condition (ii). As for the other weights, one should take $w_{1,2} = 0$, so that the limit of the action is given by $(\phi_1^2 + \phi_2^2)\tilde{\phi} + \phi_3^3 - 4\tilde{\phi}^3/27\lambda$. If one were to take $w_{1,2} > 0$, the integral of the limit would violate condition (ii), because the term $(\phi_1^2 + \phi_2^2)\tilde{\phi}$ is needed for the convergence of the integral. Then, one obtains $\Psi \sim y^{-1/3}$ in agreement with Eq. (66).

The last case is $z \to \infty$ with x, y being fixed. The leading term is

$$z\phi_1^2\phi_3. \tag{86}$$

Table 1. This table shows the asymptotic behavior of Ψ for $N = 3$ when the coefficient z of the term shown in the first column is taken to infinity. $c_{1,2}, c'_{1,2}$ are some numerical constants. The coincidence of the form between the third and the fifth rows can be understood by an orthogonal transformation $\phi_1 \to \frac{1}{\sqrt{2}}(\phi_1 + \phi_2)$, $\phi_2 \to \frac{1}{\sqrt{2}}(\phi_1 - \phi_2)$.

Term	Asymptotic behavior
$(\phi_1^2 + \phi_2^2)\phi_3$	z^{-1}
ϕ_3^3	$z^{-\frac{1}{3}}$
$(\phi_1^2 - \phi_2^2)\phi_3$	$c_1 z^{-1} + c_2 z^{-1}\log(z)$
$\phi_1^2\phi_3$	$z^{-\frac{1}{2}}$
$\phi_1\phi_2\phi_3$	$c'_1 z^{-1} + c'_2 z^{-1}\log(z)$

In a similar way to above, one can determine $w_1 = 1/2,\ w_2 = w_3 = 0$, which gives $\Psi \sim z^{-1/2}$ in agreement with Eq. (67).

The asymptotic behaviors for $N = 3$ are summarized in Table 1. In particular, there are cases, in which there exists the exceptional logarithmic correction discussed at the end of the preceding subsection.

Another simple example with non-trivial behavior is given by P with a chain-like structure:

$$P\phi^3 = |P|\left(\phi_1\phi_2^2 + \phi_2\phi_3^2 + \phi_3\phi_4^2 + \cdots + \phi_{N-1}\phi_N^2\right). \tag{87}$$

Here, since ϕ_1 is only linearly coupled, we should take $w_1 = 0$ to keep $\phi_1^2\tilde{\phi}$ of the action in the limit. As for the other ϕ_a, we should take

$$w_2 = \frac{1}{2},\ w_3 = \frac{1}{4},\ w_4 = \frac{3}{8}, \ldots, w_N = \frac{1}{3}\left(1 + (-1)^N 2^{-N+1}\right), \tag{88}$$

to cancel the overall factor $|P|$ of Eq. (87). Then, the asymptotic behavior is determined to be

$$\Psi \sim \text{const.}\,|P|^{-\sum_a w_a} = \text{const.}\,|P|^{-\frac{1}{9}\left(3N-2+(-1)^N 2^{-(N-1)}\right)}. \tag{89}$$

We have numerically checked the behavior for some small N.

As seen above, the wave function has rich asymptotic behavior depending on the direction, and how to classify all the possibilities seems an interesting non-trivial question.

8. Summary and future problems

In this paper, we have studied in some detail the profile of a wave function that exactly solves all the quantum constraints of the canonical tensor model (CTM) for general N [22]. We have found the preference for symmetric configurations, whose mechanism was described in the previous paper [23] in a general setting. This preference has been found to occur only for $\lambda > 0$, where λ is a constant in the "Hamiltonian" constraint of the CTM and is known to correspond to the cosmological constant for $N = 1$. Surprisingly, we have found some symmetries with indefinite (spacetime-like) signatures associated with the preferred configurations, not only the ones with positive definite (space-like) signatures. Since symmetries will determine the global characters of spacetimes, the results are encouraging toward showing spacetime emergence in the CTM. We have also studied the asymptotic behavior of the wave function for large values of P, and have found some rich structure.

An important technical detail in our work was to give the precise definition of the wave function, which had rather formally been given in a previous paper [22]. The wave function has the expression

of an integration over $N+1$ real variables, and the integrand oscillates infinitely fast at infinity with a constant modulus. In other words, the integral is a sort of multi-variable extension of the integral expression of the Airy function, and has conditionally convergent limits for generic values of the parameters contained in the integrand. To properly handle this rather delicate integral, we introduced a regularization, the so-called ϵ-prescription, and took its vanishing limit by properly deforming the integration contour. Then, the obtained expression of the wave function was analyzed mainly by numerical methods, as well as partly by analytical methods for simplified settings.

We have found some rich structure of the peaks and the asymptotic behavior of the wave function, which quickly become more and more complicated as N becomes larger. Our present method of analysis, which largely relies on numerical methods, cannot provide a thorough understanding of the properties of the wave function. Therefore there remain a long list of questions toward the full understanding of the quantum CTM. We considered only the particular wave function that has the most familiar Lorentzian form and is valid for general N, but there exist other possibilities of the wave functions. We would need to argue more strongly for the present particular choice of the wave function, or have to equally well consider the other possibilities in the CTM [22] and a candidate for a more fundamental model [30]. We only considered the orthogonal group symmetries with the vector representations as highlighted symmetries, but other representations and Lie groups are also possible and interesting. For example, to describe an emergent two-sphere the expected highlighted configuration would take a form like $P_{(l_1,m_1)(l_2,m_2)(l_3,m_3)} \sim \int d\omega\, Y^{m_1}_{l_1}(\omega) Y^{m_2}_{l_2}(\omega) Y^{m_3}_{l_3}(\omega)$, where $Y^m_l(\omega)$ denotes the spherical harmonics, and the irreducible representations labeled by l run from spin-zero to a cut-off. This interpretation is an area being left for later study. The other Lie groups with real orthogonal representations, which can be embedded in the $O(N)$ matrices, are also interesting to explore. The surprising appearance of spacetime signatures associated with the preferred configurations should obviously be understood more deeply. We only studied the profile of the wave function, but we rather have to perform integrations over P to evaluate physical quantities like $\int dP\, |\Psi(P)|^2 \mathcal{O}(P)$ with an observable $\mathcal{O}(P)$. By doing this we can determine whether the highlighted peaks are really physically sensible or not. This is also important to see whether the divergences at the peaks are physically harmless or not. It seems necessary to develop more effective and systematic methods to answer these questions.

Acknowledgements

The work of N.S. is supported in part by JSPS KAKENHI Grant Number 15K05050. The work of D.O. is supported in part by the Hendrik Mullerfonds. We would like to thank some of the participants for stimulating discussions at the workshop "Discrete Approaches to the Dynamics of Fields and Space-Time" held in APCTP, where the contents of this paper were presented.

Funding

Open Access funding: SCOAP[3].

Appendix A. The derivation of the wave function

In this section of the appendix, we will show the derivation of the wave function (17) [22] to make this paper self-contained. In the derivation, the validity of partial integrations is essentially important. This can be assured by taking appropriate integration contours or the appropriate prescription of regularization as taken in Sect. 4.2. The derivation of the other wave function (20) is similar. We will

also describe the result of the consistency checks of the numerical evaluation of the wave function (38), which is mentioned at the end of Sect. 4.2.

From Eqs. (12) and (15), the Hamiltonian constraint equations in the P representation are given by

$$(P_{abc}P_{bde}D^P_{cde} + \lambda_H P_{abb} - \lambda D^P_{abb})\Psi_{\rm phys}(P) = 0, \tag{A1}$$

where D^P_{abc} are the derivative operators with respect to P_{abc} with the following normalization:

$$D^P_{abc}P_{def} = \sum_\sigma \delta_{a\sigma_d}\delta_{b\sigma_e}\delta_{c\sigma_f}, \tag{A2}$$

where σ denote the permutations of d, e, and f. To get a solution, let us consider an ansatz,

$$\Psi(P) = \int_{\mathcal{C}} d\phi\, f(\phi^2)e^{iP\phi^3}, \tag{A3}$$

which was motivated by the close connection between the CTM and the randomly connected tensor networks [31–33]. Here, f denotes a function to be determined below. Applying the first operator in Eq. (A1), we obtain

$$\begin{aligned} P_{abc}P_{bde}D^P_{cde}\Psi(P) &= 6i\int_{\mathcal{C}} d\phi\; P_{abc}P_{bde}\phi_c\phi_d\phi_e f(\phi^2)e^{iP\phi^3} \\ &= 2\int_{\mathcal{C}} d\phi\; P_{abc}\phi_c f(\phi^2)\partial_b e^{iP\phi^3} \\ &= -2\int_{\mathcal{C}} d\phi\; \partial_b\left(P_{abc}\phi_c f(\phi^2)\right)e^{iP\phi^3} \\ &= -2\int_{\mathcal{C}} d\phi\; \left(P_{abb}f(\phi^2) + 2P_{abc}\phi_b\phi_c f'(\phi^2)\right)e^{iP\phi^3}, \end{aligned} \tag{A4}$$

where ∂_a denotes the derivative with respect to ϕ_a, f' the derivative of f with respect to the argument, and we have performed some partial integrations with no boundary contributions, which are assumed to be valid by appropriately taking $\mathcal{C}$. The last term of Eq. (A4) can further be computed as

$$\begin{aligned} \int_{\mathcal{C}} d\phi\; P_{abc}\phi_b\phi_c f'(\phi^2)e^{iP\phi^3} &= \frac{1}{3i}\int_{\mathcal{C}} d\phi\, f'(\phi^2)\partial_a e^{iP\phi^3} \\ &= \frac{2i}{3}\int_{\mathcal{C}} d\phi\; \phi_a f''(\phi^2)e^{iP\phi^3}. \end{aligned} \tag{A5}$$

Now let us assume

$$f''(x) = Axf(x) \tag{A6}$$

with a numerical constant A. Then, the last expression in Eq. (A5) can further be computed as

$$\begin{aligned} \int_{\mathcal{C}} d\phi\; \phi_a f''(\phi^2)e^{iP\phi^3} &= A\int_{\mathcal{C}} d\phi\; \phi_a\phi^2 f(\phi^2)e^{iP\phi^3} \\ &= \frac{A}{6i}D^P_{abb}\int_{\mathcal{C}} d\phi\, f(\phi^2)e^{iP\phi^3}. \end{aligned} \tag{A7}$$

Finally, by collecting the expressions above, we obtain an identity satisfied by $\Psi(P)$:

$$\left[P_{abc}P_{bde}D^P_{cde} + 2P_{abb} + \frac{4A}{9}D^P_{abb}\right]\Psi(P) = 0. \tag{A8}$$

This identity implies that a solution to Eq. (A1) is given by Eq. (18), if we put

$$A = -\frac{9}{4}\lambda. \tag{A9}$$

As for Eq. (A6), the solution is given by the Airy function, and an integral expression of f can be given by

$$f(x) = \int_{\tilde{\mathcal{C}}} d\tilde{\phi}\ \exp\left[i\left(x\tilde{\phi} + \frac{\tilde{\phi}^3}{3A}\right)\right] \tag{A10}$$

with an appropriate integration contour $\tilde{\mathcal{C}}$. By putting this expression into the ansatz (A3), we obtain Eq. (17).

Let us finally check the momentum constraints. Similarly, by performing some partial integrations, we obtain

$$\begin{aligned}
\hat{\mathcal{J}}_{ab}\Psi(P) &= (P_{acd}D^P_{bcd} - P_{bcd}D^P_{acd})\int_{\mathcal{C}} d\phi\, f(\phi^2)e^{iP\phi^3} \\
&= 6i\int_{\mathcal{C}} d\phi\, f(\phi^2)(P_{acd}\phi_b\phi_c\phi_d - P_{bcd}\phi_a\phi_c\phi_d)e^{iP\phi^3} \\
&= 2i\int_{\mathcal{C}} d\phi\, f(\phi^2)(\phi_b\partial_a - \phi_a\partial_b)e^{iP\phi^3} \\
&= -2i\int_{\mathcal{C}} d\phi\ \left(\partial_a(f(\phi^2)\phi_b) - \partial_b(f(\phi^2)\phi_a)\right)e^{iP\phi^3} \\
&= 0.
\end{aligned} \tag{A11}$$

This proves that Ψ_{phys} satisfies the momentum constraints.

The integration region of the wave function considered in the text is a real plane, and hence the integrand does not damp at infinity. Nonetheless, the integration converges conditionally for generic P, because the integrand oscillates infinitely fast at the infinity of the integration region. As in Sect. 4, we treat this delicate integration by introducing the so-called ϵ-prescription, which is often used in physics to regularize, and finally take the $\epsilon \to +0$ limit. In this case, the above proof cannot be applied to the wave function, since there exists an extra contribution to the identity (A8) from the regularization term. In general, it is not a trivial question whether the extra contribution vanishes in the vanishing limit of the regularization, but the present case is easy to answer as follows. If we add the regularization term, $-\epsilon\phi^2 - \epsilon\tilde{\phi}^2$, to the exponent of Eq. (A3), the additional term to Eq. (A8) turns out to be

$$\epsilon\int_{\mathbb{R}^{N+1}} d\phi d\tilde{\phi}\ \left(c_1 P_{abc}\phi_b\phi_c + c_2\phi_a\tilde{\phi}\right)e^{i\left(P\phi^3+\phi^2\tilde{\phi}-\frac{4}{27\lambda}\tilde{\phi}^3\right)-\epsilon\phi^2-\epsilon\tilde{\phi}^2} \tag{A12}$$

with numerical constants c_1, c_2. This vanishes in the $\epsilon \to 0^+$ limit for generic P, because, irrespective of the additional function of $\phi, \tilde{\phi}$ in the integrand, the integration is still conditionally convergent due to the infinitely fast oscillations of the integrand at infinity, and the overall factor ϵ will make the breaking term vanish.

The above argument supports the validity of the ϵ-prescription taken in the text. As explained in Sect. 4.2, the $\epsilon \to +0$ limit requires a deformation of the integration contour that should not change the values of the wave function due to the Cauchy theorem, if the deformation parameter Δ is small enough. To be sure, we performed some direct numerical checks of our method of computing

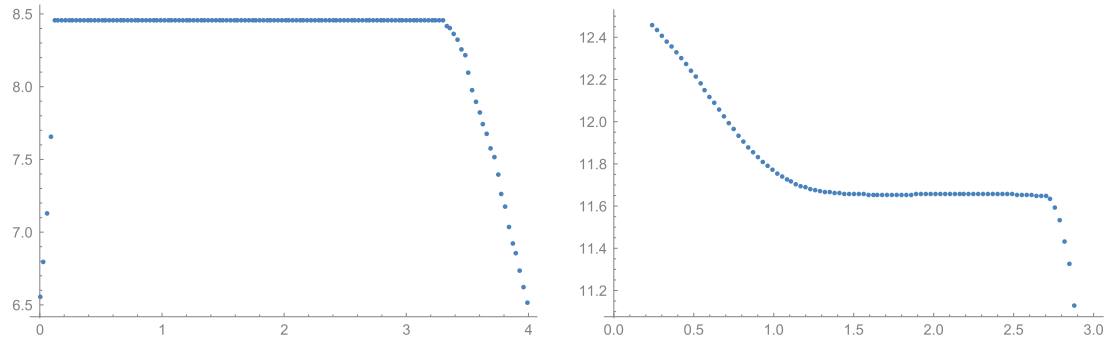

Fig. A1. The dependence of the numerical values of the wave function (38) on Δ. The left is for $N = 2$ and $\lambda = 1$ at a "generic" configuration $(P_{111}, P_{112}, P_{122}, P_{222}) = (1, 1.1, 1.2, 1.3)$, and the right for $N = 3$ and $\lambda = 1$ at $(P_{111}, P_{112}, \ldots, P_{333}) = (1.0111, 1.0222, 1.0333, \ldots, 1.111)$. The horizontal axis represents $-\log_{10}(\Delta)$, and the vertical axis the wave function. There exist substantial regions of constant values, which are supposed to be the real values of the wave function.

Eq. (38). We studied the dependence of the wave function on Δ for $N = 1, 2, 3$. Two of the results are shown in Fig. A1. As shown, the graphs contain substantial regions of constancy, the values of which can be regarded as the real values of the wave function in the vanishing limit of the regularization. The deviations in the left region (larger Δ) should come from the fact that the deformed contours cross some branch cuts or singularities. The deviations in the right region (smaller Δ) come from the fact that the deformed contour is so close to the singularities that the numerical integrations suffer from errors.

Another check was to see whether the key identity (A8) is satisfied by the numerically computed wave function. We have obtained some satisfactorily small numbers of the violations for $N = 1, 2, 3$. For example, we obtained the violation of order $\sim 10^{-8}$ for $N = 2$ and $\Delta = 0.1$, and $\sim 10^{-2}$ for $N = 3$ and $\Delta = 10^{-1.8}$, respectively, for the same parameters used in Fig. A1. Though it is hard to judge whether these numbers can be regarded as zero, we also observed the tendency that the violations became smaller when the optional parameters of the numerical integration command were chosen to produce more precise numerical values.

In the checks above, several hours of computation time were needed even for $N = 3$ to get the satisfactorily precise results shown in Fig. A1.[22] However, the slow speed to get precise values is not so problematic for our main purpose. This is because we are not interested in the values themselves, but in the qualitative behavior of the wave function to see the highlighting phenomenon of symmetric configurations. Therefore, in most cases, we can set the optional parameters in favor of the speed, sacrificing unnecessary preciseness.

Appendix B. The difficulty of the $\lambda = 0$ wave functions

In this appendix, we will explain the difficulty of the wave functions for $\lambda = 0$, namely Eq. (17) with $\lambda = 0$ and Eq. (20).

[22] We performed the numerical computation with Mathematica 11. The optional parameters of the numerical integration command had to be tuned to get better results. In our computation, it was important to make the option value "MaxErrorIncreases" at least several tens of thousands, while its default value is two thousand.

Let us first consider Eq. (17). By a change of variable $\tilde{\phi} \to |\lambda|^{1/3}\tilde{\phi}$ and taking the limit $\lambda \to 0$, one can see that ϕ and $\tilde{\phi}$ are decoupled. P is coupled only with ϕ, and the wave function is given by

$$\Psi(P) = \int_{\mathbb{R}^N} d\phi \, e^{iP\phi^3}. \tag{B1}$$

By considering a rescaling of variables $\phi \to |P|^{-1/3}\phi$, it is obvious that the wave function splits into radial and angular parts as

$$\Psi(P) = |P|^{-\frac{N}{3}}\Psi(P_\Omega), \tag{B2}$$

where we have introduced a polar coordinate with $P_{\Omega\, abc} = P_{abc}/|P|$. Then, from Eqs. (14) and (18), the physical wave function is given by

$$\Psi_{\rm phys}(P) = |P|^{-\frac{N(N+2)(N+3)}{12}}\Psi(P_\Omega)^{\frac{(N+2)(N+3)}{4}}. \tag{B3}$$

Therefore, the wave function has a strong peak at the origin $P \sim 0$. To be more precise, let us include the volume factor as well:

$$\int dP \, |\Psi_{\rm phys}(P)|^2 = \int \frac{d|P|}{|P|} dP_\Omega \, |P|^{-\frac{N(N+2)}{3}} |\Psi(P_\Omega)|^{\frac{(N+2)(N+3)}{2}}, \tag{B4}$$

where we have used the fact that the dimension of the space of P is given by $N(N+1)(N+2)/6$. Therefore, $P = 0$ is the most favorable configuration, which would have the physical meaning that there are no spaces.

This preference for $P = 0$ is qualitatively understandable, because, at $P = 0$, the integrand does not depend on ϕ and the integration trivially diverges. Similar reasoning can also be applied not only to this global preference, but to the partial cases in which the configurations with $P_{abc} = 0$, $\exists a, \forall b, c$ are relatively preferred, because then the integrand does not depend on ϕ_a, and the integration over ϕ_a diverges. Therefore, generally speaking, the configurations with less effective N are preferred. This tendency to collapse will make it hard for the case of $\lambda = 0$ to be physically sensible.

Let us turn to Eq. (20). In a similar manner, we obtain

$$\Psi(Q) = |Q|^{-\frac{N+2\alpha}{3}}\Psi(Q_\Omega), \tag{B5}$$

where $\alpha = (N+3)(N-2)/8$. Then,

$$\int dQ \, |\Psi(Q)|^2 = \int \frac{d|Q|}{|Q|} dQ_\Omega \, |Q|^{\frac{N^3+2N^2-3N+6}{6}} |\Psi(Q_\Omega)|^2. \tag{B6}$$

Since the exponent is positive for $N \geq 1$, the wave function diverges at infinity. This problem of this case seems be a "conjugate dual" to the former one: the wave function spreads out to infinity. It would be difficult to physically make sense of this case as well.

Appendix C. A simple expression of the calculable model

The integral that we want to consider here is

$$\Psi = \int_{\mathbb{R}^{N+1}} \prod_{j=1}^{N} d\phi_j d\tilde{\phi} \exp\left(iS(\phi, \tilde{\phi}, x, y) - \epsilon(\phi^2 + \tilde{\phi}^2)\right), \tag{C1}$$

where $\epsilon > 0$, $\phi^2 = \sum_{i=1}^{N} \phi_i^2$, and

$$S(\phi, \tilde{\phi}, x, y) = \sum_{i=1}^{N-1} x_i \phi_i^2 \phi_N + y\phi_N^3 + \phi^2\tilde{\phi} - k\tilde{\phi}^3 \tag{C2}$$

with $k = \frac{4}{27\lambda}$.

There are two difficult things in the actual evaluation of this integration. One is the multi-variable integration, and the other is the $\epsilon \to +0$ limit. We will reduce the former to a single integration, and safely take the latter by deforming the integration contour of the remaining single integration.

By doing the Gaussian integrations over ϕ_i $(i = 1, 2, \ldots, N-1)$, one obtains

$$\Psi = \pi^{\frac{N-1}{2}} \int_{\mathbb{R}^2} d\phi d\tilde{\phi} \prod_{j=1}^{N-1} \frac{1}{\sqrt{\epsilon - i(x_j\phi + \tilde{\phi})}} \exp\left(i\left(\phi^2\tilde{\phi} + y\phi^3 - k\tilde{\phi}^3\right) - \epsilon(\phi^2 + \tilde{\phi}^2)\right), \tag{C3}$$

where ϕ_N has been replaced by ϕ for notational simplification.

By dividing the integration region of ϕ into positive and negative regions, the wave function (C3) can be expressed as

$$\Psi = \pi^{\frac{N-1}{2}} (A_+ + A_-), \tag{C4}$$

where

$$A_+ = \int_0^\infty d\phi \int_{-\infty}^\infty d\tilde{\phi} \prod_{j=1}^{N-1} \frac{1}{\sqrt{\epsilon - i(x_j\phi + \tilde{\phi})}} \exp\left(i\left(\phi^2\tilde{\phi} + y\phi^3 - k\tilde{\phi}^3\right) - \epsilon(\phi^2 + \tilde{\phi}^2)\right),$$

$$A_- = \int_{-\infty}^0 d\phi \int_{-\infty}^\infty d\tilde{\phi} \prod_{j=1}^{N-1} \frac{1}{\sqrt{\epsilon - i(x_j\phi + \tilde{\phi})}} \exp\left(i\left(\phi^2\tilde{\phi} + y\phi^3 - k\tilde{\phi}^3\right) - \epsilon(\phi^2 + \tilde{\phi}^2)\right). \tag{C5}$$

One can easily show that $A_+^* = A_-$ by performing a change of variables, $\phi \to -\phi, \tilde{\phi} \to -\tilde{\phi}$. Therefore,

$$\Psi = 2\pi^{\frac{N-1}{2}} \mathrm{Re}\left[A_+\right]. \tag{C6}$$

To compute A_+, let us perform a change of variable, $\tilde{\phi} \to \phi\tilde{\phi}$. Then, we obtain

$$A_+ = \int_0^\infty d\phi \int_{-\infty}^\infty d\tilde{\phi} \prod_{j=1}^{N-1} \frac{1}{\sqrt{\epsilon - i(x_j + \tilde{\phi})}} \phi^{1-\frac{N-1}{2}} \exp\left(-\left(\epsilon - i\left(\tilde{\phi} + y - k\tilde{\phi}^3\right)\right)\phi^3\right), \tag{C7}$$

where we have used the positivity of ϕ. Here, the regularization parameter ϵ has been replaced, keeping the same roles as in Eq. (C5), namely, a suppression term at infinity and the choice of the branches of the square roots. However, the replacement introduces a new singularity at $\phi = 0$, as can be seen in the power of ϕ in the integrand of Eq. (C7).

As mentioned above, the integration (C7) has a divergence at the endpoint $\phi = 0$ for positive N. This singularity did not exist in the original integration before the replacement of the regularization parameter, and therefore has to be regulated in another way. One way is to consider an analytic

continuation of N from negative to positive values. Then, by formally carrying out the ϕ integration, one obtains

$$A_+ = \frac{1}{3}\Gamma\left(\frac{5-N}{6}\right)\int_{-\infty}^{\infty} d\tilde{\phi}\prod_{j=1}^{N-1}\frac{1}{\sqrt{\epsilon - i(x_j+\tilde{\phi})}}\left(\epsilon - ih(\tilde{\phi})\right)^{\frac{N-5}{6}}, \tag{C8}$$

where

$$h(\tilde{\phi}) = \tilde{\phi} + y - k\tilde{\phi}^3. \tag{C9}$$

Here, the remaining $\tilde{\phi}$ integration is convergent, because the integrand behaves like $\sim \tilde{\phi}^{-2}$ as it tends to infinity.

In Eq. (C8), the regularization parameter ϵ determines how to take the integration contour in relation to the branch cuts of the integrand. By using the Cauchy theorem, one can take the $\epsilon \to 0^+$ limit by continuously deforming the integration contour $\mathcal{C}$ away from the real plane. Here, the fractional powers of the integrand in Eq. (C8) are supposed to be taken in the main branches. Hence, the branch cuts associated with $\tilde{\phi} = -x_i$ extend in the direction of the negative pure imaginary, as in Fig. 4. If we first consider the case that $(N-5)/6$ is fractional, there also exist branch cuts associated with the solutions to $h(\tilde{\phi}) = 0$. The relevant solutions are those on the real axis, and the branch cuts extend from there to the negative or positive imaginary regions, depending on whether the signs of $h'(\tilde{\phi})$ at the solutions are positive or negative, respectively. The contour $\mathcal{C}$ should be taken so as to circumvent those branch cuts. An example is shown in Fig. 4. With this understanding of the integration contour $\mathcal{C}$, one obtains an ϵ-free expression:

$$A_+ = \frac{1}{3}\Gamma\left(\frac{5-N}{6}\right)\int_{\mathcal{C}} d\tilde{\phi}\prod_{j=1}^{N-1}\frac{1}{\sqrt{-i(x_j+\tilde{\phi})}}\left(-ih(\tilde{\phi})\right)^{\frac{N-5}{6}}. \tag{C10}$$

When $n = (N-5)/6$ is a non-negative integer, Eq. (C10) cannot be used, because the overall factor (the gamma function) is divergent. Moreover, in this case, the integrand has no singularities in the positive imaginary region, and one can deform $\mathcal{C}$ to infinity to show that the integration vanishes because of the fast damping behavior $\tilde{\phi}^{-2}$ of the integrand. Thus, the expression (C10) is actually indeterministic, $\Psi = \infty \cdot 0$.

To resolve this issue, let us take the analytic continuation in N more carefully. Let us consider a perturbation of N as $N = 6n + 5 + 6\alpha$ with an infinitesimal α. The relevant formulas are

$$\begin{aligned}\Gamma\left(\frac{5-N}{6}\right) &= \frac{(-1)^{n+1}}{n!\,\alpha} + \cdots,\\ (\epsilon - ih)^{n+\alpha} &= (\epsilon - ih)^n e^{\alpha \ln(\epsilon - ih)} = (\epsilon - ih)^n(1 + \alpha\ln(\epsilon - ih) + \cdots).\end{aligned} \tag{C11}$$

Putting these into Eq. (C10) and taking the zeroth order in α (the lowest-order α^{-1} vanishes because of the vanishing of the integration explained above), one obtains

$$A_+ = \frac{(-1)^{n+1}}{3n!}\int_{\mathcal{C}} d\tilde{\phi}\prod_{j=1}^{N-1}\frac{1}{\sqrt{-i(x_j+\tilde{\phi})}}\left(-ih(\tilde{\phi})\right)^n \ln\left(-ih(\tilde{\phi})\right), \tag{C12}$$

where the integration contour is taken in the same manner as previously.

The formula (C6) with Eqs. (C10) and (C12) was numerically compared with the computation based on the generally applicable method (but rather slow due to the multi-variable integration) explained in Sect. 4.2. We have found perfect agreement in all the cases that we checked up to $N = 5$, supporting the validity of the derivation of the formula.

Appendix D. Normalizability of the wave function in the large-P region

In this appendix, we will discuss the normalizability of the wave function in the large-P region, when the wave function has the asymptotic behavior that can be derived from the scaling argument discussed in Sect. 7. This appendix does not fully prove the normalizability of the wave function in the large-P region, because we assume the scaling argument, which we know does not cover all the cases, as shown in Sect. 7. Therefore, this appendix proves the normalizability only in part of the large-P region, which we expect should cover most of the configuration space.

As discussed in Sect. 7, the scaling argument assumes the existence of a scaling of ϕ_a that satisfies conditions (i) and (ii). One can easily derive the following set of necessary conditions for (i) and (ii):

$$\begin{aligned} &w_a + w_b + w_c \geq 1 \text{ if } P_{abc} \neq 0, \ \forall a, b, c, \\ &w_a + w_b + w_c = 1, \ \exists a, b, c, \\ &w_a \geq 0, \ \forall a. \end{aligned} \tag{D1}$$

The first one is necessary for condition (i), because, after the rescaling of ϕ, the term $P_{abc}|P|^{-w_a-w_b-w_c}\phi_a\phi_b\phi_c$ in the action should not diverge in the asymptotic limit $|P| \to \infty$. The third one is necessary for the same reason for $|P|^{-2w_a}\phi_a^2\tilde{\phi}$ in the action. The second one is necessary for condition (ii), because at least one triple term must remain in the action in the asymptotic limit for the convergence of the integral. Here, note that it is not possible to keep all the $\phi_a^2\tilde{\phi}$ terms in the action in the asymptotic limit for assuring the convergence of the integral, because the first one of Eq. (D1) requires that at least one of w_a must be positive.

As shown in Appendix A, the physical wave function is given by Eq. (18) with Eq. (14):

$$\Psi_{\text{phys}}(P) = \Psi(P)^{\frac{1}{4}(N+2)(N+3)}, \tag{D2}$$

where Ψ is the wave function (17). Therefore, if we assume the scaling argument, the asymptotic behavior of Ψ_{phys} is given by

$$\Psi_{\text{phys}} \sim \text{const.}\, |P|^{-\frac{1}{4}(N+2)(N+3)\sum_{a=1}^{N} w_a}, \tag{D3}$$

where we have used Eq. (83).

Now, let us consider perturbations δP_{abc} of P_{abc}, and qualitatively estimate the allowed range of the perturbations under the requirement that the asymptotic behavior keeps the same form (D3) with a given set $\{w_a;\ a = 1, 2, \ldots, N\}$. First of all, if the perturbations δP_{abc} of P_{abc} satisfy $\delta P_{abc}|P|^{-(w_a+w_b+w_c)} \to 0$ in $|P| \to \infty$, the limiting action after the rescaling does not change. Therefore, in this case, the wave function keeps the same asymptotic form as Eq. (D3) including the overall constant. We can consider more general perturbations. Because of (ii), the limiting action can be perturbed by certain finite amounts without losing the convergence of the integral. Such perturbations are on the order of $\delta P_{abc} \sim |P|^{w_a+w_b+w_c}$. In this case, the overall constant in Eq. (D3) can change, because it is determined by the integration value with the limiting action, while the scaling behavior in $|P|$ keeps the same form. Thus we obtain the following qualitative estimation of

the range of perturbations that are allowed for the asymptotic behavior determined by a given set $\{w_a;\ a = 1, 2, \ldots, N\}$:

$$\delta P_{abc} \lesssim |P|^{w_a+w_b+w_c}. \tag{D4}$$

Then, the contribution to the norm of $\Psi_{\rm phys}$ from such a region, denoted below by $P_{\{w\}}$, can be estimated as

$$\begin{aligned}
||\Psi_{\rm phys}||^2_{P_{\{w\}}} &= \int_{P_{\{w\}}} \prod_{\substack{a,b,c=1\\ a\le b\le c}}^{N} dP_{abc}\ |\Psi_{\rm phys}|^2 \\
&\lesssim \int \frac{d|P|}{|P|} \left(\prod_{\substack{a,b,c=1\\ a\le b\le c}}^{N} |P|^{w_a+w_b+w_c} \right) |P|^{-\frac{1}{2}(N+2)(N+3)\sum_{a=1}^N w_a} \\
&= \int \frac{d|P|}{|P|} |P|^{-(N+2)\sum_{a=1}^N w_a} \\
&\le \int \frac{d|P|}{|P|} |P|^{-\frac{1}{3}(N+2)} < \infty.
\end{aligned} \tag{D5}$$

Here, from the first to the second lines, we have used Eq. (D3) and the range (D4), and also the first line of Eq. (D1) for the radial direction; from the second to the third lines, we have used the fact that each w_a appears $\frac{1}{2}(N+1)(N+2)$ times in the product; and from the third to the last lines, we have used $\sum_{a=1}^N w_a \ge \frac{1}{3}$, which can be proved from Eq. (D1). The estimate (D5) shows that $\Psi_{\rm phys}$ is normalizable in the large-P region of $P_{\{w\}}$.

Note that the estimation above does not prove the normalizability of the wave function in the large-P region. The obstacle is that we do not know exactly to what extent all the $P_{\{w\}}$ cover the whole large-P region, since we know that our scaling argument does not cover all the possible asymptotic behavior, as shown in Sect. 7. What we have shown in this appendix is merely that the normalizability of the wave function in the large-P region is assured at least in the vicinities of P with the asymptotic behavior consistent with the scaling argument. On the other hand, the result of this appendix seem to narrow down the possibilities of the breakdown of the normalizability in the large-P region to the following two kinds of locations: the boundaries between different asymptotic regions, and the vicinities of the exceptional cases to our scaling argument. Though the discussions in this appendix are qualitative and partial, they will at least give good guidance in more thorough future study.

References

[1] M. H. Goroff and A. Sagnotti, Nucl. Phys. B **266**, 709 (1986).
[2] N. Sasakura, Mod. Phys. Lett. A **06**, 2613 (1991).
[3] J. Ambjørn, B. Durhuus, and T. Jónsson, Mod. Phys. Lett. A **06**, 1133 (1991).
[4] N. Godfrey and M. Gross, Phys. Rev. D **43**, R1749(R) (1991).
[5] I. R. Klebanov and G. Tarnopolsky, J. High Energy Phys. **10**, 037 (2017) [arXiv:1706.00839 [hep-th]] [Search INSPIRE].
[6] R. Gurau, Commun. Math. Phys. (2017), doi: 10.1007/s00220-017-3055-y [arXiv:1706.05328 [hep-th]] [Search INSPIRE].
[7] R. Gurau, Commun. Math. Phys. **304**, 69 (2011) [arXiv:0907.2582 [hep-th]] [Search INSPIRE].
[8] E. Witten, arXiv:1610.09758 [hep-th] [Search INSPIRE].
[9] I. R. Klebanov and G. Tarnopolsky, Phys. Rev. D **95**, 046004 (2017) [arXiv:1611.08915 [hep-th]] [Search INSPIRE].

[10] R. Gurau and J. P. Ryan, Ann. Henri Poincaré **15**, 2085 (2014) [arXiv:1302.4386 [math-ph]] [Search INSPIRE].
[11] V. Bonzom, R. Gurau, A. Riello, and V. Rivasseau, Nucl. Phys. B **853**, 174 (2011) [arXiv:1105.3122 [hep-th]] [Search INSPIRE].
[12] J. Ambjørn, J. Jurkiewicz, and R. Loll, Phys. Rev. Lett. **93**, 131301 (2004) [arXiv:hep-th/0404156] [Search INSPIRE].
[13] J. Ambjørn, A. Görlich, J. Jurkiewicz, and R. Loll, Phys. Rept. **519**, 127 (2012) [arXiv:1203.3591 [hep-th]] [Search INSPIRE].
[14] D. N. Coumbe and J. Laiho, J. High Energy Phys. **04**, 028 (2015) [arXiv:1401.3299 [hep-th]] [Search INSPIRE].
[15] J. Laiho, S. Bassler, D. Coumbe, D. Du, and J. T. Neelakanta, Phys. Rev. D **96**, 064015 (2017) [arXiv:1604.02745 [hep-th]] [Search INSPIRE].
[16] N. Sasakura, Int. J. Mod. Phys. A **27**, 1250020 (2012) [arXiv:1111.2790 [hep-th]] [Search INSPIRE].
[17] R. Arnowitt, S. Deser, and C. W. Misner, Gen. Relat. Gravit. **40**, 1997 (2008) [arXiv:gr-qc/0405109] [Search INSPIRE].
[18] N. Sasakura and Y. Sato, Phys. Lett. B **732**, 32 (2014) [arXiv:1401.2062 [hep-th]] [Search INSPIRE].
[19] N. Sasakura and Y. Sato, J. High Energy Phys., **10**, 109 (2015) [arXiv:1506.04872 [hep-th]] [Search INSPIRE].
[20] H. Chen, N. Sasakura, and Y. Sato, Phys. Rev. D **95**, 066008 (2017) [arXiv:1609.01946 [hep-th]] [Search INSPIRE].
[21] N. Sasakura, Int. J. Mod. Phys. A **28**, 1350111 (2013) [arXiv:1305.6389 [hep-th]] [Search INSPIRE].
[22] G. Narain, N. Sasakura, and Y. Sato, J. High Energy Phys. **01**, 010 (2015) [arXiv:1410.2683 [hep-th]] [Search INSPIRE].
[23] D. Obster and N. Sasakura, Eur. Phys. J. C **77**, 783 (2017) [arXiv:1704.02113 [hep-th]] [Search INSPIRE].
[24] R. M. Wald, *General Relativity* (University of Chicago Press, Chicago, IL, 1984).
[25] A. Ashtekar, Phys. Rev. Lett. **57**, 2244 (1986).
[26] T. Thiemann, *Modern Canonical Quantum General Relativity* (Cambridge University Press, Cambridge, UK, 2007), Cambridge Monographs on Mathematical Physics.
[27] N. Sasakura, Int. J. Mod. Phys. A **27**, 1250096 (2012) [arXiv:1203.0421 [hep-th]] [Search INSPIRE].
[28] C. J. Howls, Proc. R. Soc. Lond. A **453**, 2271 (1997).
[29] E. Witten, AMS/IP Stud. Adv. Math. **50**, 347 (2011) [arXiv:1001.2933 [hep-th]] [Search INSPIRE].
[30] G. Narain and N. Sasakura, Classical Quantum Gravity **34**, 145009 (2017) [arXiv:1612.04938 [hep-th]] [Search INSPIRE].
[31] N. Sasakura and Y. Sato, Prog. Theor. Exp. Phys. **2015**, 043B09 (2015) [arXiv:1501.05078 [hep-th]] [Search INSPIRE].
[32] N. Sasakura and Y. Sato, SIGMA **10**, 087 (2014) [arXiv:1402.0740 [hep-th]] [Search INSPIRE].
[33] N. Sasakura and Y. Sato, Prog. Theor. Exp. Phys. **2014**, 053B03 (2014) [arXiv:1401.7806 [hep-th]] [Search INSPIRE].